

Review

# A Review of Activation Persulfate by Iron-Based Catalysts for Degrading Wastewater

Keke Zhi <sup>1,\*</sup>, Zhe Li <sup>2</sup> , Pengfei Ma <sup>2</sup>, Yongxiang Tan <sup>1</sup>, Yuefeng Zhou <sup>1</sup>, Weikang Zhang <sup>1</sup> and Jingxing Zhang <sup>2</sup>

<sup>1</sup> Department of Engineering, China University of Petroleum-Beijing at Karamay, Karamay 834000, China; tanyongxian@163.com (Y.T.); 2020015534@st.cupk.edu.cn (Y.Z.); 2020015530@st.cupk.edu.cn (W.Z.)

<sup>2</sup> Department of Petroleum, China University of Petroleum-Beijing at Karamay, Karamay 834000, China; 2020015113@st.cupk.edu.cn (Z.L.); 2020015117@st.cupk.edu.cn (P.M.); 2020015130@st.cupk.edu.cn (J.Z.)

\* Correspondence: zhikeke@cupk.edu.cn

**Abstract:** Advanced oxidation technology of persulfate is a new method to degrade wastewater. As the economy progresses and technology develops, increasingly more pollutants produced by the paper industry, printing and dyeing, and the chemical industry are discharged into water, causing irreversible damage to water. Methods and research directions of activation persulfate for wastewater degradation by a variety of iron-based catalysts are reviewed. This review describes the merits and demerits of advanced oxidation techniques for activated persulfate by iron-based catalysts. In order to promote the development of related research work, the problems existing in the current application are analyzed.

**Keywords:** iron-based catalysts; activation persulfate; degrading wastewater



**Citation:** Zhi, K.; Li, Z.; Ma, P.; Tan, Y.; Zhou, Y.; Zhang, W.; Zhang, J. A Review of Activation Persulfate by Iron-Based Catalysts for Degrading Wastewater. *Appl. Sci.* **2021**, *11*, 11314. <https://doi.org/10.3390/app112311314>

Academic Editor: Maria Gavrilescu

Received: 29 October 2021

Accepted: 26 November 2021

Published: 29 November 2021

**Publisher's Note:** MDPI stays neutral with regard to jurisdictional claims in published maps and institutional affiliations.



**Copyright:** © 2021 by the authors. Licensee MDPI, Basel, Switzerland. This article is an open access article distributed under the terms and conditions of the Creative Commons Attribution (CC BY) license (<https://creativecommons.org/licenses/by/4.0/>).

## 1. Introduction

With people's yearning for a better life, increasingly more new materials are used in the petrochemical, medical, and pharmaceutical industries. As a result, huge amounts of organic pollutants are produced [1–3]. Advanced oxidation processes (AOPs) can generate a variety of free radical ions, which can gradually decompose large organic matter into small organic matter until mineralization occurs. At present, advanced oxidation methods include Fenton oxidation [4–6], ozone oxidation [7,8], photolysis [9–11], photocatalysis [12,13], and ferrate (VI) catalytic oxidation [14–16], etc. It is worth mentioning that advanced oxidation technology (sulfate radical-based AOPs, SR-AOPs) based on persulfate (PS) that can produce sulfate radical ion ( $\text{SO}_4^-$ ) is also attracting increasing attention [17,18].

In recent years, sulfonamides antibiotics (SAs) have been widely detected in urban and agricultural wastewater and its receiving water in many regions of the world [19], and it is estimated that about 12 t of sulfamethoxazole (SMX) is discharged into the South China Sea via the Mekong River every year [20]. When it enters the water body, it affects the survival and growth of the microbial community and microfauna, and even induces antibiotic resistance, which will eventually destroy the virtuous cycle of the entire ecosystem [21]. SR-AOPs have shown a great result in this regard [22,23]. This technology not only has a good effect in the treatment of antibiotic wastewater, but also shows excellent performance in the treatment of oilfield wastewater [24].

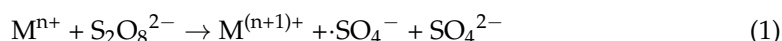
Common persulfates include peroxymonosulfate (peroxymonosulfate, PMS) and peroxydisulfate (peroxydisulfate, PDS). Owing to the high redox potential (2.5–3.1 V) [25] of the sulfate radical ion, it can effectively oxidize organic pollutants into  $\text{H}_2\text{O}$  and  $\text{CO}_2$  as a powerful oxidant. It can also be applied over a wide range of pH, from 3 to 8 [22,26,27]. Although PS is a strong oxidant, without the action of catalyst the number of collisions with organic pollutants is reduced, which greatly reduces the effect of the chemical agent [28].

Iron is a transition metal, less toxic than copper and manganese. At present, there are many reports about the application of various [29] iron-based catalysts such as  $\text{CuFe}_2\text{O}_4$  [30–32] in the activation of persulfate [33–35]. In this paper, the role of various iron-based catalysts in the activation of persulfate is reviewed. Then, we introduce the advanced oxidation technology of persulfate, as well as the current problems and development prospects, so as to promote the sustainable development of this technology.

## 2. Activation Persulfate by Various Iron-Based Catalysts

### 2.1. $\text{MeFe}_2\text{O}_4$ ( $\text{Me} = \text{Cu}, \text{Co}, \text{Zn}, \text{etc.}$ )

In terms of activation mechanism, transition metal compounds react with PS to produce a large amount of  $\cdot\text{SO}_4^-$ ; the reaction equation follows:



As can be seen from the above reaction, metal ions are in a free state dispersed in the solution during the reaction process. Although the wastewater can be degraded by the activation persulfate mechanism, it belongs to homogeneous catalysis; metal ions will be dissolved in the aqueous solution, which causes difficult separation from solution. Therefore, the production cost is greatly increased due to its difficult recycling nature, and it is easy to cause secondary pollution to the environment. Therefore,  $\text{MeFe}_2\text{O}_4$  with a low metal leaching rate has become a new research direction. Through PS/PMS [36] heterogeneous catalytic technology, these problems can be effectively solved [22,37,38].

At present, there are several common methods for preparing iron-based catalysts: hydrothermal, solvothermal, sol–gel preparation, and coprecipitation methods.

In the hydrothermal method, the solute is dispersed into the solution, stirred, and heated in the reactor, and finally washed and dried to obtain the required product [39].

Similar to the hydrothermal method, the solvothermal method changes water into an organic solvent. By dissolving one or more precursors in a nonaqueous solvent, the reaction occurs in liquid phase or supercritical conditions [40].

The sol–gel method is to dissolve the metal alkoxides in organic solvents, form homogeneous solutions, add other components, react at a certain temperature to form gels, and finally make products by drying [41].

Coprecipitation is an important method to prepare composite oxide ultrafine powder containing a large variety of metal elements [42].

The electron transfer between transition metal oxides is much higher [43] than that between single transition metal oxides. Generally,  $\text{AB}_2\text{O}_4$  [44,45] structure is referred to as spinel structure.  $\text{CuFe}_2\text{O}_4$  is a typical spinel ferrite with a magnetic structure, which has high chemical stability and low metal leaching rate. Taking  $\text{CuFe}_2\text{O}_4$  as an example, compared with single transition metal oxides, Fe and Cu elements can play a role in the reaction; respectively, they can also activate PS to produce  $\cdot\text{OH}$  and  $\cdot\text{SO}_4^-$ .

G. Xian et al. [46] comprehensively compared the catalytic degradation effects of  $\text{CoFe}_2\text{O}_4$ ,  $\text{CuFe}_2\text{O}_4$ ,  $\text{MnFe}_2\text{O}_4$ , and  $\text{ZnFe}_2\text{O}_4$ . In detail,  $\text{CuFe}_2\text{O}_4$  presented the best and fastest catalytic performance in organics removal. Almost 87.6% azo dye acid orange 7 (AO7) was removed in PS solution coupled with  $\text{CuFe}_2\text{O}_4$  [46]. Additionally, it was known that  $\text{CuFe}_2\text{O}_4$  had the best catalytic effect. Moreover, through the quenching experiment, it was not  $\cdot\text{OH}$  but  $\cdot\text{SO}_4^-$  that played a major role in the reaction.

Table 1 shows the degradation effects of some different  $\text{MeFe}_2\text{O}_4$ -activated PS/PMS on different kinds of wastewater. It can be seen from the table that the iron-based catalyst with spinel structure mainly acts on  $\cdot\text{SO}_4^-$  in the mechanism of activation persulfate; the effect of  $\cdot\text{OH}$  is slightly worse [47]. Of course, there are also some nonfree radical pathways, which degrade pollutants in water by generating singlet oxygen  $^1\text{O}_2$  [48–50].

**Table 1.** Effect of Different MeFe<sub>2</sub>O<sub>4</sub>-activated PMS on degradation of different wastewater [39–42,47,51–53].

Catalyst	Pollution	Main Mechanism	Pollutant Concentration	Catalyst Concentration	Oxidant	Oxidation Concentration	T/min	Degradation Rate/%	Number of Cycles	Synthesis Techniques	Ref.
PbFe <sub>2</sub> O <sub>4</sub>	Thionine	<sup>1</sup> O <sub>2</sub>	10 μM	0.4 g/L	PMS	400 μM	20	100	Not mentioned	Solution combustion	[51]
CoFe <sub>2</sub> O <sub>4</sub> -loaded quartz sand	Sulfachloropyridazine sodium	·SO <sub>4</sub> <sup>-</sup> ·OH	2 g/L	10 g	PMS	75 mg/L	150	90	Not mentioned	Citrate combustion	[52]
CoFe <sub>2</sub> O <sub>4</sub> -SAC	Norfloxacin (NOF)	·SO <sub>4</sub> <sup>-</sup> ·OH	10 mg/L	0.1 g/L	PMS	0.15 g/L	120	TOC reduction 81	5 (>80%)	Hydrothermal	[47]
The biochar loaded with CoFe <sub>2</sub> O <sub>4</sub> nanoparticles	Bisphenol A (BPA)	·SO <sub>4</sub> <sup>-</sup> ·OH	10 mg/L	0.05 g/L	PMS	0.5 g/L	8	93	Not mentioned	Hydrothermal	[39]
C <sub>3</sub> N <sub>4</sub> @MnFe <sub>2</sub> O <sub>4</sub> -graphene	Metronidazole	·SO <sub>4</sub> <sup>-</sup> ·OH	20 mg/L	1.0 g/L	PS	0.01 M	90	94.5	5 (>80%)	Solvothermal	[40]
Zn <sub>0.8</sub> Cu <sub>0.2</sub> Fe <sub>2</sub> O <sub>4</sub>	Atrazine	·SO <sub>4</sub> <sup>-</sup>	4.4 μM	200 mg/L	PS	0.5 mM	30	95	Not mentioned	Sol-gel	[41]
CuFe <sub>2</sub> O <sub>4</sub> /O <sub>3</sub>	2,4-Dichlorophenoxyacetic acid (2,4-D)	Not mentioned	20 mg/L	0.20 g/L	PMS O <sub>3</sub>	PMS 2.0 mM; O <sub>3</sub> 16.0 mg/L;	40	88.9	5 (>80%)	Coprecipitation	[42]
CoFe <sub>2</sub> O <sub>4</sub>	Atrazine (ATZ)	·SO <sub>4</sub> <sup>-</sup>	10 mg/L	0.4 g/L	PMS	0.8 mM	30	>99	5 (>60%)	Hydrothermal	[53]

## 2.2. $\text{MeFe}_2\text{O}_4$ Combined with the Carrier

As mentioned above, the carrier recombination method can increase the specific surface area and increase the contact of chemical sites [54], thus greatly improving the rate of chemical reaction. At present,  $\text{SiO}_2$  [54,55], black phosphorus [56,57], and rGO [58,59] (reduced graphene oxide) are commonly used as carriers. After compositing with the carrier, it is closely combined with the carrier by van der Waals force [58] or electrostatic interaction [60], making it difficult to fall off the surface of the carrier.

Pure graphene is a benzene-ring-like two-dimensional nanomaterial consisting of  $\text{sp}^2$  hybrid orbitals. However, its high production cost limits its large-scale application. Afterward, by improving Hummer's method, a large number of oxygen-containing functional groups were linked at the edge of the plane by a strong oxidant, hence the name GO (graphene oxide) (Figure 1); rGO (Figure 2) was obtained by sodium borohydride and other means of reduction, which has low synthesis cost and is suitable for use as a good carrier of catalysis.

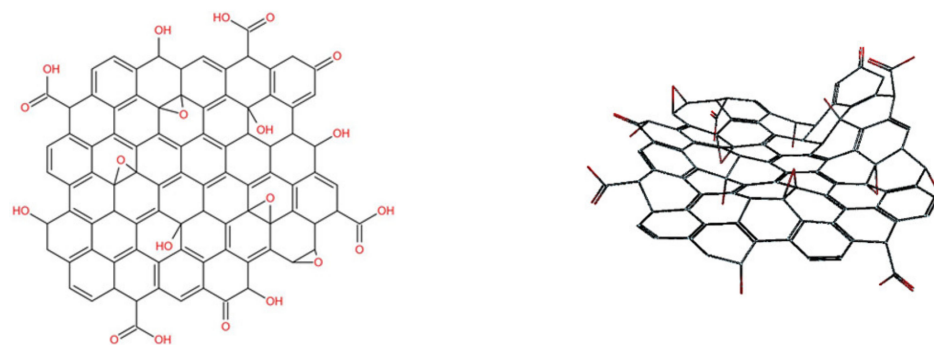


**Figure 1.** Plane structure (left) and solid structure (right) of GO (bond line type).



**Figure 2.** Plane structure (left) and solid structure (right) of rGO (bond line type).

Taking  $\text{CuFe}_2\text{O}_4$ , a representative of  $\text{MeFe}_2\text{O}_4$ , as an example, by comparing the effect of pure  $\text{CuFe}_2\text{O}_4$  with that of  $\text{CuFe}_2\text{O}_4$  combined with the carrier, it can be seen that the latter has a stronger catalytic effect under acidic and photoinduced conditions [61].  $\text{CuFe}_2\text{O}_4$  in  $\text{CuFe}_2\text{O}_4$ -rGO is closely combined with the oxygen-containing groups on rGO through electrostatic interaction, as shown in Figure 3. Images from a scanning electron microscope are shown in Figure 4.

Table 2 shows the degradation effects of some  $\text{CuFe}_2\text{O}_4$  and rGO composite materials on different kinds of wastewater. It can be seen from the table that the composite catalyst can still produce good effects even without the presence of PS. Not only the Cu, Fe, and other elements in the catalyst can produce pure chemical catalytic effect, but the carrier rGO can produce electron transition under the light condition, promoting the transfer of electrons, and plays a part of the photocatalytic effect [62,63]. Table 2 contains some other carriers, which can also greatly influence degradation of different kinds of wastewater.

**Table 2.** Effects of partial  $\text{MeFe}_2\text{O}_4$  and carrier composite materials on degradation of different kinds of wastewater [61,64–70].

Catalyst	Pollution	Main Mechanism	Pollutant Concentration	Catalyst Concentration	Oxidant	Oxidation Concentration	T/min	Degradation Rate /%	Number of Cycles	Synthesis Techniques	Ref.
$\text{CuFe}_2\text{O}_4$ -20%rGO	Methylparaben	$\text{SO}_4^{\cdot-}$ $\cdot\text{OH}$	10 mg/L	0.2 mg/L	PS	5 mM	120	96	Not mentioned	Sol-gel	[64]
$\text{CuFe}_2\text{O}_4$ -1% (w/w) rGO	Phenol	$\cdot\text{OH}$	20 ppm	5 mL	30% $\text{H}_2\text{O}_2$	6 mg/L	240	100	Not mentioned	Coprecipitation	[61]
$\text{CuFe}_2\text{O}_4/\text{g-C}_3\text{N}_4$	Propranolol	$\text{SO}_4^{\cdot-}$	0.02 mM	1 g/L	PS	1 mM	120	82.2	Not mentioned	Sol-gel	[65]
$\text{CoFe}_2\text{O}_4/\text{CCNF}$	Dimethyl phthalate	$\text{SO}_4^{\cdot-}$	0.05 mM	0.5 g/L	PMS	1.5 mM	60	>90	5 (>90%)	Sol-gel	[66]
$\text{TiO}_2@\text{CuFe}_2\text{O}_4/\text{UV}$	2,4-D	$\text{SO}_4^{\cdot-}$	20 mg/L	0.1 g/L	PMS	0.3 mM	60	97.2	5 (>90%)	Sol-gel	[67]
$\text{ZnS-ZnFe}_2\text{O}_4$	Rhodamine B	$\text{SO}_4^{\cdot-}$	20 mg/L	20 mg	PS	5 mg	90	97.67	3 (>95%)	Hydrothermal	[68]
$\text{Fe}_2\text{O}_3@\text{CoFe}_2\text{O}_4$	NOF	$\text{SO}_4^{\cdot-}$ $\cdot\text{OH}$	15 $\mu\text{M}$	0.3 g/L	PMS	0.4 mM	25	89.8	4 (90%)	Hydrothermal	[69]
Nitrogen and sulfur codoped CNTs-COOH loaded $\text{CuFe}_2\text{O}_4$	2-Phenylbenzimidazole-5-sulfonic acid	$\text{SO}_4^{\cdot-}$	5 mg/L	50 mg/L	PMS	1:100 (molar ratio)	40	98	5 (>95%)	Coprecipitation	[70]

@: the composite of two materials.

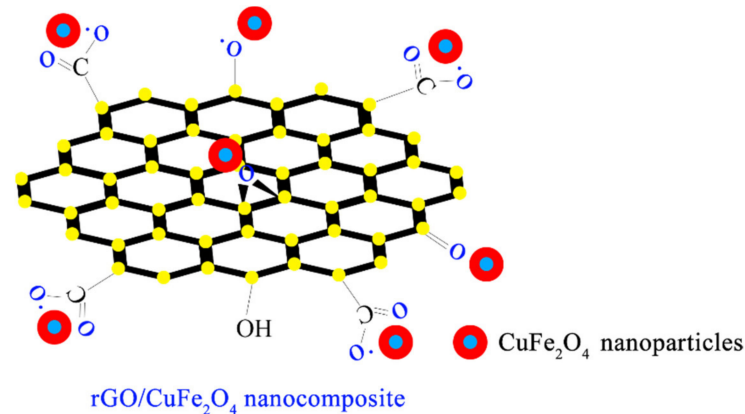


Figure 3. Chemical structural formula of CuFe<sub>2</sub>O<sub>4</sub>-rGO [60].

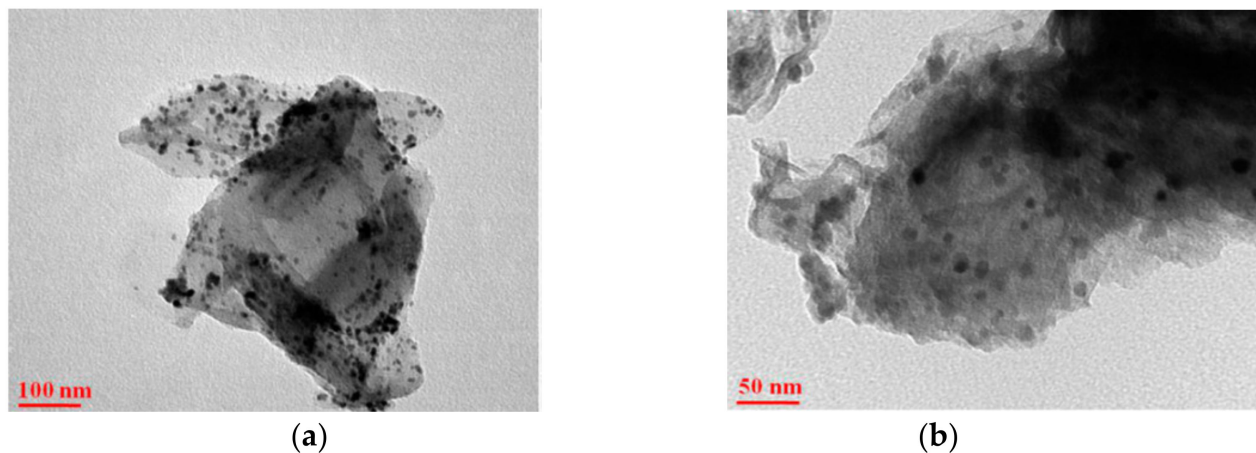
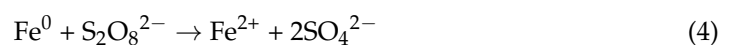


Figure 4. TEM images of (a,b) rGO/CuFe<sub>2</sub>O<sub>4</sub> nanostructures under different magnifications [60].

### 2.3. Activation Persulfate by Fe<sup>0</sup>

In recent years, activation persulfate based on Fe<sup>0</sup> (zero-valent iron, ZVI) have been widely used in chemical production and environmental remediation [71,72]. As mentioned above, the activation persulfate/Fe (II) mechanism can cause secondary pollution to water, so ZVI/PS [73,74] is used instead to reduce a series of problems caused by the reduction of Fe<sup>2+</sup> content due to the change of pH and other factors in water [71].

ZVI/PS system has strong reducibility (Fe<sup>0</sup>, E<sup>0</sup> = −0.44 V) [75]. Compared with CuFe<sub>2</sub>O<sub>4</sub>, its reaction process is more complex, as shown in Figure 5. Fe<sup>0</sup> is first converted to Fe<sup>2+</sup> in the presence of acid and oxidant, then further oxidized to Fe<sup>3+</sup> by Fe<sup>2+</sup>, and finally to Fe(IV) [76,77]. The reaction mechanism follows [78]: According to the reaction equation, the reaction is easily affected by pH, and the reaction will gradually slow with the increase of pH. Weng et al. [79] point out that the Fe<sup>0</sup>/PS system exhibits two-stage kinetics. The kinetic first stage is mostly attributed to a heterogeneous reaction occurring on the surface of the Fe<sup>0</sup> aggregate. As the reaction proceeds, decolorization shifts from the slow kinetic first stage to the fast kinetic second stage when sufficient Fe<sup>2+</sup> ions are maintained in the system [80].



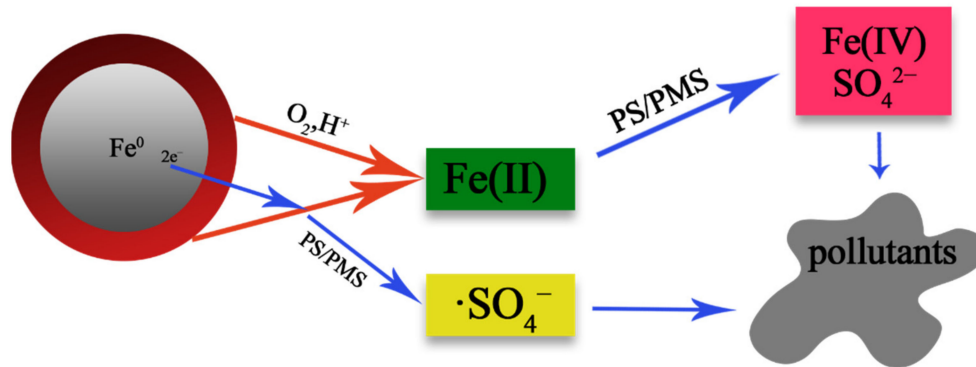
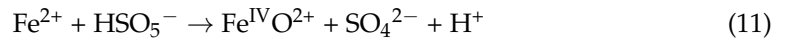
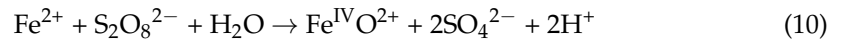
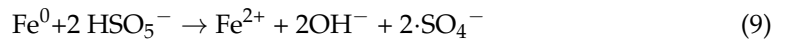
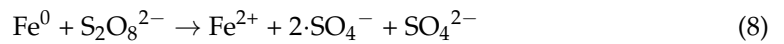
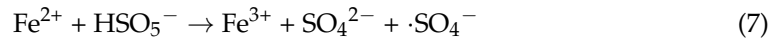
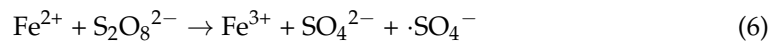


**Figure 5.** Schematic of the formation of  $\cdot\text{SO}_4^-$  and Fe(IV) in nZVI/persulfate systems containing methyl phenyl sulfoxide [81].

Figure 6 shows the proposed degradation pathway of 2,4-D [82]. By examining Figure 6, it can further confirm that macromolecular organic matter is decomposed into small molecular organic matter, which is gradually mineralized.

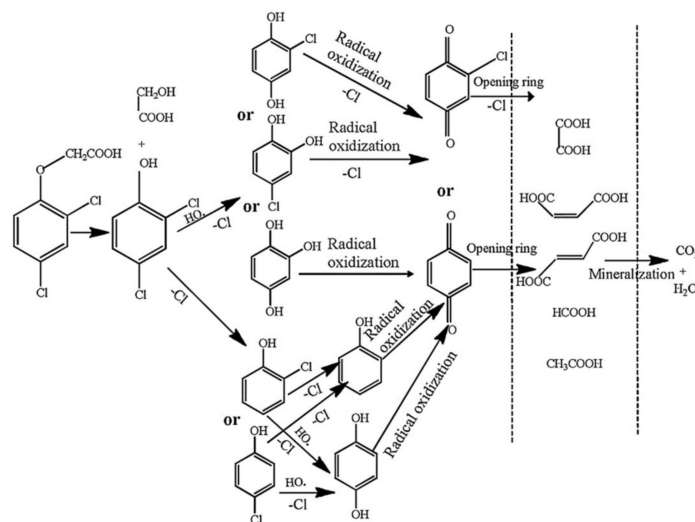


**Figure 6.** The proposed degradation pathway of 2,4-D [82].

Table 3 shows the degradation effects of various types of polluted water bodies activated by PS/PMS based on elemental iron. Usually, an appropriate amount of  $\text{H}_2\text{O}_2$  [83] will be added to the water when PS is activated by  $\text{Fe}^0$ , so as to reduce the cost of oxidant. Through the analysis of the table, it can be seen that the effect of ZVI when used alone [84] is worse than when it is combined with the carrier or when other conditions exist.

**Table 3.** Degradation effect of different kinds of wastewater based on PS/PMS activated by different kinds of iron [85–92].

Catalyst	Pollution	Main Mechanism	Pollutant Concentration	Catalyst Concentration	Oxidant	Oxidation Concentration	T/min	Degradation Rate /%	Number of Cycles	Synthesis Techniques	Ref.
nZVI	Sulfamethazine	$\cdot\text{OH}$ $\cdot\text{SO}_4^-$	50 mg/L	2 mM	PS $\text{H}_2\text{O}_2$	1 mM 0.5 mM	30	96	Not mentioned	Sol-gel	[88]
CN-Fe	Sulfamethazine	$\cdot\text{OH}$ $^1\text{O}_2$	50 $\mu\text{M}$	0.5 g/L	PMS	1 mM	15	82	Not mentioned	Carbothermal	[87]
Carbon-coated nZVI	4-chlorophenol	$\cdot\text{SO}_4^-$ $\cdot\text{OH}$	150 $\mu\text{M}$	0.25 g/L	PMS	1 mM	120	96	Not mentioned	Commercially available	[86]
US-nZVI	Chloramphenicol	$\cdot\text{SO}_4^-$ $\cdot\text{OH}$	5 mg/L	0.5 g/L	PMS	1 mM	90	98.1	Not mentioned	Liquid phase reduction	[85]
$\text{Fe}^0/\text{Fe}_3\text{O}_4$	Dibutyl phthalate	$\cdot\text{OH}$ $\cdot\text{SO}_4^-$	18 $\mu\text{M}$	0.5 g L <sup>-1</sup>	PS	1.8 mM	180	94.7	6 (>68%)	Calcination	[89]
$\text{Fe}^0/\text{Fe}_3\text{O}_4$	Atrazine	$\cdot\text{OH}$ $\cdot\text{SO}_4^-$	500 $\mu\text{g}/\text{L}$	25 mg/L	PMS	1 mM	2	100	Not mentioned	Reduction	[90]
Fe@C	Bisphenol S	$\cdot\text{OH}$ $\cdot\text{SO}_4^-$	5 mg/L	0.5 g/L	PMS	1.0 mM	60	92.8	Not mentioned	Resin carbonization	[91]
Fe@C/PB	2,4-DichloroPhenol	$\cdot\text{OH}$ $\cdot\text{SO}_4^-$	20 mg/L	0.6 g/L	PMS	2.0 g/L	50	99.4	Not mentioned	Calcination	[92]

@: the composite of two materials.

### 2.4. Fe<sub>3</sub>O<sub>4</sub>

Fe<sub>3</sub>O<sub>4</sub> magnetite, also known as magnetic iron oxide, is a black crystal with a rotating spinel structure (Figure 7). In magnetite, Fe<sup>2+</sup> and Fe<sup>3+</sup> are disordered on the ferrite octahedron, so electrons can transfer rapidly between Fe<sup>2+</sup> and Fe<sup>3+</sup>; thus, reversible redox reactions can occur at the same position on the octahedron.

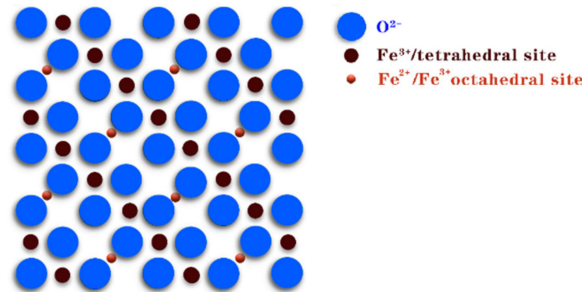


Figure 7. Crystal structure of Fe<sub>3</sub>O<sub>4</sub>.

However, since Fe<sub>3</sub>O<sub>4</sub> is easy to accumulate in solution and contact sites are reduced after agglomeration, single Fe<sub>3</sub>O<sub>4</sub> is rarely used. Using the composite carrier method [93] can not only solve these problems, but also speeds the reaction rate, making it more cost effective when applied in industrial production. He et al. [94] pointed out that the Fe<sub>3</sub>O<sub>4</sub>/GO/Ag composite microspheres are formed using magnetic Fe<sub>3</sub>O<sub>4</sub> as cores, followed by coating an internal layer of GO and an outer layer of Ag nanoparticles, as Figure 8 shows. The synthesized Fe<sub>3</sub>O<sub>4</sub>/GO/Ag composite catalyst under the action of NaBH<sub>4</sub>, methylene blue, and ciprofloxacin can be completely degraded within 12 min. Figure 8 shows SEM images of Fe<sub>3</sub>O<sub>4</sub>/GO/Ag composite catalyst. In Figure 9, we can clearly observe that Ag has been completely attached to the Fe<sub>3</sub>O<sub>4</sub>/GO surface, which can increase the specific surface area and improve the chemical reaction rate.

Table 4 shows the research progress of Fe<sub>3</sub>O<sub>4</sub> and its composite materials on the degradation of different pollutants reported at present. According to the data in the table, when Fe<sub>3</sub>O<sub>4</sub> is compounded with the carrier, the catalytic performance is greatly improved.

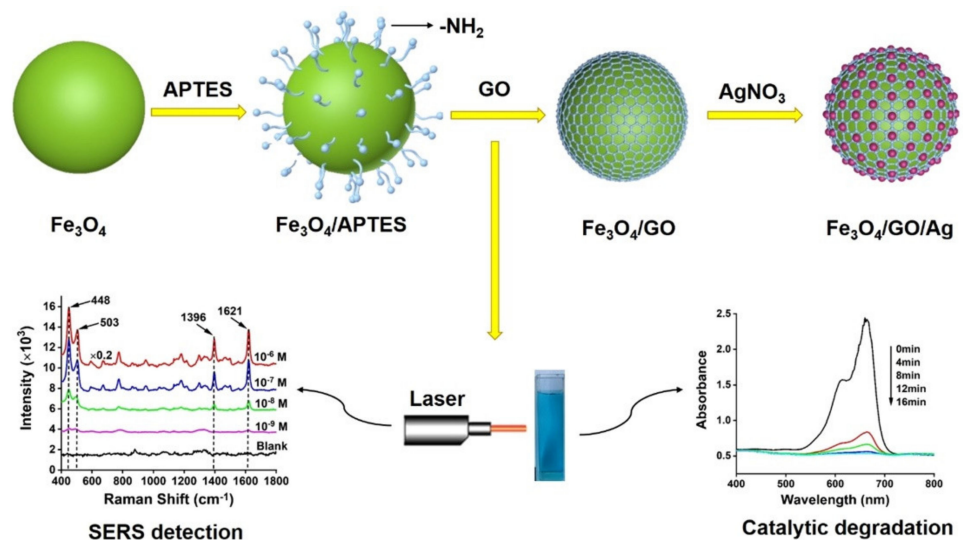
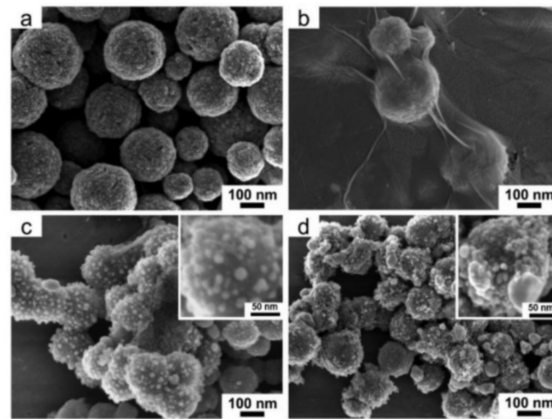


Figure 8. Illustration of the fabrication of Fe<sub>3</sub>O<sub>4</sub>/GO/Ag composite microspheres [94].

**Table 4.** Effects of Fe<sub>3</sub>O<sub>4</sub> and its composite-material-activated PS/PMS on degradation of different kinds of wastewater [95–101].

Catalyst	Pollution	Main Mechanism	Pollutant Concentration	Catalyst Concentration	Oxidant	Oxidation Concentration	T/min	Degradation Rate /%	Number of Cycles	Synthesis Techniques	Ref.
Fe <sub>3</sub> O <sub>4</sub>	BPA	·SO <sub>4</sub> <sup>−</sup> ·OH	20 mg/L	2.0 g/L	PMS	5 mM	30	27.53	Not mentioned	Commercially available	[95]
CuO-Fe <sub>3</sub> O <sub>4</sub> -BC	BPA	·SO <sub>4</sub> <sup>−</sup> ·OH	20 mg/L	2.0 g/L	PMS	5 mM	30	100	4 (>85%)	Coprecipitation	[96]
rGO-Fe <sub>3</sub> O <sub>4</sub>	NOF	<sup>1</sup> O <sub>2</sub> ·OH ·SO <sub>4</sub> <sup>−</sup>	20 mg/L	0.5 g/L	PS	1 g/L	30	89.69	Not mentioned	Coprecipitation	[96]
Fe <sub>3</sub> O <sub>4</sub>	Sulfamonomethoxine	·SO <sub>4</sub> <sup>−</sup>	0.06 mM	2.4 mM	PS	1.2 mM	15	100	Not mentioned	Coprecipitation	[97]
Fe <sub>3</sub> O <sub>4</sub> @Zn/Co-ZIFs	Carbamazepine	·SO <sub>4</sub> <sup>−</sup>	5 mg/L	25 mg/L	PMS	0.4 mM	30	100	Not mentioned	Solvothermal	[98]
Fe <sub>3</sub> O <sub>4</sub> /microwave irradiation (3 kW/L)	p-Nitrophenol	·SO <sub>4</sub> <sup>−</sup>	20 mg/L	2.5 g/L	PS	15:1 (molar ratio)	28	94.2	Not mentioned	Not mentioned	[99]
Fe <sub>3</sub> O <sub>4</sub> /MC	p-Hydroxybenzoic acid	·SO <sub>4</sub> <sup>−</sup>	1.0 g/L	0.2 g/L	PS	1.0 g/L	30	100	Not mentioned	Sol-gel	[100]
Fe <sub>3</sub> O <sub>4</sub> /graphene aerogels	Malachite green	Not mentioned	20 mg/L	0.2 g/L	PS	1.0 mM	12	91.7	Not mentioned	Sol-gel	[101]

@: the composite of two materials.



**Figure 9.** Typical FESEM images of (a)  $\text{Fe}_3\text{O}_4$ , (b)  $\text{Fe}_3\text{O}_4/\text{GO}$ , (c)  $\text{Fe}_3\text{O}_4/\text{GO}/\text{Ag}$ , and (d)  $\text{Fe}_3\text{O}_4/\text{Ag}$  microspheres. Inserts are magnified FESEM images of  $\text{Fe}_3\text{O}_4/\text{GO}/\text{Ag}$  and  $\text{Fe}_3\text{O}_4/\text{Ag}$  microspheres [94].

### 3. Comparison of the Performance of Different Iron-Based Catalysts

Different catalysts and contaminants are described above. We select representative pollutants, 2,4-D, NOF, and BPA, as examples to illustrate the performance of various kinds of catalysts.

As one type of auxin analogue, 2,4-D is the most applied herbicides in the world. If overused, it pollutes the water body and harms crops [102]. Figure 10 shows that when the concentration of 2,4-D was 20 mg/L, all three iron-based catalysts showed excellent degradation rate and fast degradation time. The best material is  $\text{Fe}@C/\text{PB}$ , which can degrade 99.4% of the 2,4-D in 50 min [92].

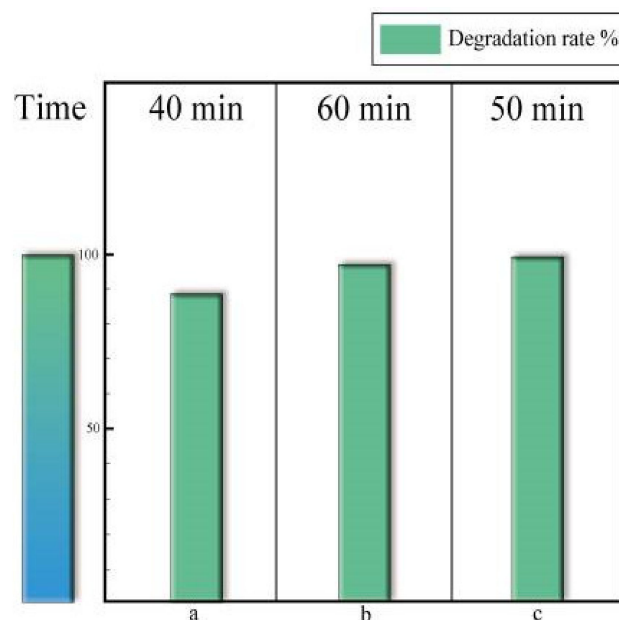


**Figure 10.** Degradation of 2,4-D by three iron-based catalysts: (a)  $\text{CuFe}_2\text{O}_4/\text{O}_3$  [42], (b)  $\text{TiO}_2@\text{CuFe}_2\text{O}_4/\text{UV}$  [69], and (c)  $\text{Fe}@C/\text{PB}$  [92].

Antibiotics are currently extensively used in human medicine, animal farming, agriculture, and aquaculture, and their residue has become a global environmental problem [103]. NOF is the third generation of quinolone antibiotic. It has certain antibacterial action [104]. Figure 12 shows that when the concentration of NOF was 15  $\mu\text{M}$ ,  $\text{Fe}_2\text{O}_3@\text{CoFe}_2\text{O}_4$  was 0.3 g/L. In 25 min, the degradation rate could reach 89.8% [69]. Compared with the degra-

degradation rate of other pollutants, it has a greater improvement. Piezoelectric catalysis can be used to further enhance performance.

BPA is a very common chemical product. It is widely found in plastics used in our daily life. It can lead to endocrine disorders, and cancer is also considered to be associated with BPA [105]. Figure 11 shows that when the concentration of BPA was 10 mg/L, the degradation rate of (a) the biochar loaded with  $\text{CoFe}_2\text{O}_4$  nanoparticles can reach 93% [39] in 8 min.

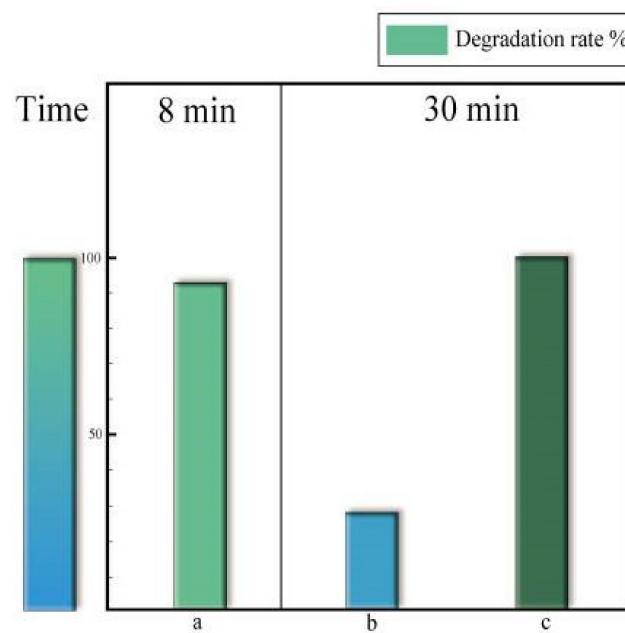


**Figure 11.** Degradation of BPA by three iron-based catalysts: (a) biochar loaded with  $\text{CoFe}_2\text{O}_4$  nanoparticles [39], (b)  $\text{Fe}_3\text{O}_4$  [87], and (c)  $\text{CuO-Fe}_3\text{O}_4\text{-BC}$  [88].

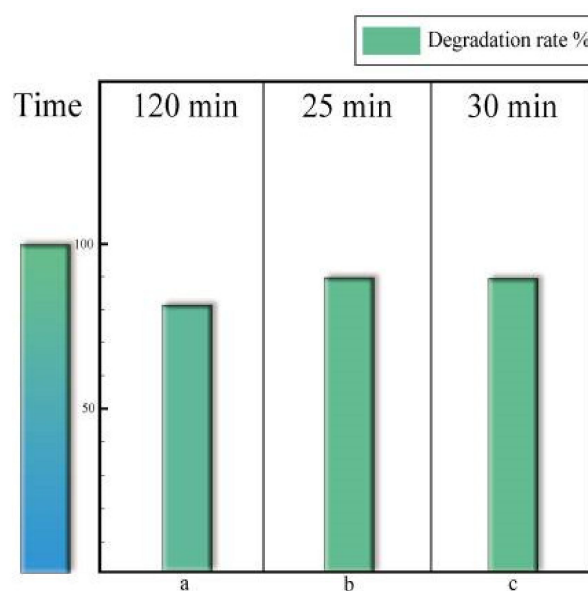
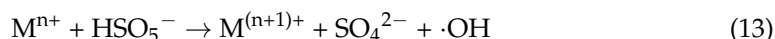
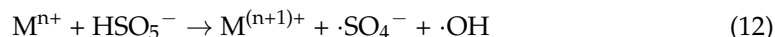


**Figure 12.** Degradation of NOF by three iron-based catalysts: (a)  $\text{CoFe}_2\text{O}_4\text{-SAC}$  [47], (b)  $\text{Fe}_2\text{O}_3@\text{CoFe}_2\text{O}_4$  [69], and (c)  $\text{rGO-Fe}_3\text{O}_4$  [88].

## 4. Coupling Activation of Iron-Based Catalysts under Auxiliary Action

### 4.1. Photocatalytic Activation

Transition metal compounds with lower states can effectively activate PMS, and the reaction mechanism follows:



Currently, photocatalytic activation of PS can be done either through direct exposure to ultraviolet light, or through the reaction of light with the photocatalyst to excite the photoinduced electrons on its surface [106]. According to many studies, the efficiency of Fenton-like degradation of pollutants by iron-based catalyst can be improved under the condition of light [107,108]. As an efficient catalyst to activate persulfate, Fe<sup>2+</sup> also shows good performance under dark conditions, but there are still problems such as the reduction of utilization rate caused by the mutual transformation of Fe<sup>2+</sup> and Fe<sup>3+</sup>. Benkelberg et al. [109] found in their study that under ultraviolet light, the transformation of Fe<sup>3+</sup> into Fe<sup>2+</sup> in the solution was accelerated, and the Fe(OH)<sub>2</sub> generated by the reaction would greatly absorb ultraviolet light and produce Fe<sup>2+</sup> and ·OH. The reaction mechanism follows:



However, as described above, homogeneous catalysis based on Fe<sup>2+</sup> is prone to many problems. Therefore, heterogeneous catalysis based on an iron catalyst is relatively more convenient to recycle and is environmentally friendly. Regardless of the form the iron-based catalyst enters the solution, it will be converted to Fe<sup>2+</sup> to activate PS and degrade the pollutants in the water. It is Fe<sup>2+</sup> that plays a vital role in activating persulfate. Part of the ions converted to Fe<sup>3+</sup> will also be converted to Fe<sup>2+</sup> through illumination and other ways to speed the reaction process.

Table 5 shows the degradation effects of different iron-based catalysts on different pollutants under UV lamp irradiation. The data in the Table show that the degradation effect is the best under UV lamp irradiation (UV-Vis) within the visible range.

**Table 5.** Effects of different iron-based catalysts on degradation of different pollutants under ultraviolet lamp irradiation [107,110–115].

Catalyst	Pollution	Pollutant Concentration	Catalyst Concentration	Oxidant	Oxidation Concentration	T/min	Degradation Rate /%	Number of Cycles	Synthesis Techniques	Ref.
UV/Fe <sup>2+</sup>	Lindane	3.43 mM	50 mM	PMS	250 mM	180	92.2	Not mentioned	Commercially available	[110]
CuO-UV/Fe <sub>2</sub> O <sub>3</sub>	2,4-D	50 mg/L	0.5 g/L	PMS	3 mM	60	90.2	Not mentioned	Hydrothermal	[111]
UV-Vis/Fe(II)	Carbamazepine	0.05 mM	0.1 mM	PMS	0.2 mM	30	100	Not mentioned	Commercially available	[112]
UV/Fe <sup>2+</sup>	Lindane	3.43 mM	0.25 mM	PMS	0.25 mM	720	78.4	Not mentioned	Commercially available	[110]
UV/Fe <sup>2+</sup>	Atrazine	18.56 μM	17.91 μM	PS	1856 μM	Not mentioned	62.94	Not mentioned	Commercially available	[107]
UV-Vis/Fe(II)	Diclofenac, Sulfamethoxazole	Compound = 50 μM	1 mM	PMS	2 mM	60	>70	Not mentioned	Commercially available	[113]
Vis/ZnFe <sub>2</sub> O <sub>4</sub>	Orange II	20 mg L <sup>-1</sup>	0.1 g L <sup>-1</sup>	PMS	0.5 g L <sup>-1</sup>	80	100	Not mentioned	Commercially available	[114]
Vis/ZnFe <sub>2</sub> O <sub>4</sub>	Orange II	100 mg L <sup>-1</sup>	0.5 g L <sup>-1</sup>	PS	1.0 g L <sup>-1</sup>	300	50.5	5 (95%)	Sol-gel	[115]

### 4.2. Piezoelectric Catalytic Activation

Piezoelectrics are a noncentrosymmetric crystal structure that separates positive and negative charges under the action of external forces, resulting in a corresponding piezopotential [116–118]. Piezocatalysis refers to the conversion of mechanical energy into chemical energy. When using an iron-based catalyst piezoelectric material or coupled with other photocatalysts, an electric field near the piezoelectric material assists in charge separation [119].

Vibration is a very common motion that produces mechanical energy. Compared with commonly used oxidation methods such as Fenton reaction and photoelectric catalysis, piezoelectric catalytic activation is more resource-saving. Even a very small vibration can drive a deformation of nano/micrometer materials to generate a potential [120]. The degradation mechanism of piezoelectric catalysis follows [121]:



Ultrasound (US) is the most common wave that can generate mechanical energy. PS is converted into  $\cdot\text{SO}_4^-$  under the action of ultrasound; the reaction equation follows [122]:



The study of Xu et al. [123] indicated that in the ultrasonic environment, activation persulfate based on foamed zero-valent iron ( $\text{Fe}^0_f$ ) could remove the oxide film on the surface of  $\text{Fe}^0_f$  in the reaction process. Thus, more  $\text{Fe}^0_f$  is exposed to the solution to increase the contact area and speeds the reaction. In the persulfate/chlorite  $\text{Fe}^0_f$  system, a large number of  $\cdot\text{SO}_4^-$ ,  $\cdot\text{OH}$  and other free radical ions can be generated through ultrasonic action. The possible reaction mechanism is shown in Figure 13 [123].

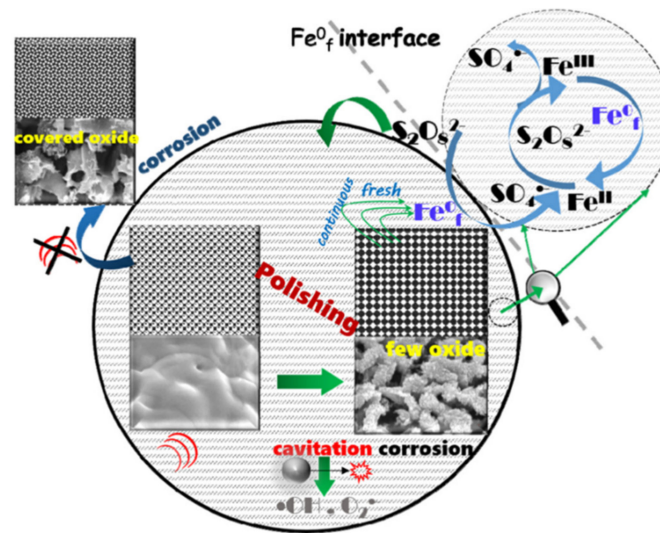


Figure 13. The possible reaction mechanism of US/ $\text{Fe}^0_f$ -PS [123].

As an activation method of piezoelectric catalysis, an ultrasonic wave is partially used as an example in the Table 6 to degrade different kinds of wastewater through the activation persulfate mechanism.

**Table 6.** Under the action of ultrasound, iron-based catalysts degrade different kinds of wastewater by activation persulfate [37,88,123–128].

Catalyst	Condition of US	Pollution	Pollutant Concentration	Catalyst Concentration	Oxidant	Oxidation Concentration	T/min	Degradation Rate /%	Number of Cycles	Synthesis Techniques	Ref.
US/PS/ Fe <sup>0</sup> <sub>f</sub>	30 W L <sup>-1</sup> 28 kHz	Tmp <sub>FG</sub>	50 μM	0.214 mM	PS	1.45 mM	40	100	Not mentioned	Commercially available	[123]
US/ Fe <sup>0</sup>	140 W L <sup>-1</sup>	SD	20 mg/L	1.3 mM	PS	1.3 mM	30	97.4	Not mentioned	Hydrothermal	[124]
US/ Fe <sup>0</sup>	60 W L <sup>-1</sup>	SMT	0.05 mM	0.1 mM	PS	1 mM	30	100	Not mentioned	Magnetization	[125]
US/Fe <sup>2+</sup> (pH = 3.5)	40 kHz	Azorubine	20 mg L <sup>-1</sup>	4 mM	PS	4 mM	60	66.5	Not mentioned	Commercially available	[126]
US/Fe <sub>3</sub> O <sub>4</sub>	20 kHz	Azo dye	0.06 mM	0.4 g/L	PMS	3 mM	30	90	Not mentioned	Hydrothermal	[127]
US/nZVI	360 W L <sup>-1</sup> 40 kHz	Chloramphenicol	5 mg/L	0.5 g/L	PS	1 mM	90	98.1	Not mentioned	Hydrothermal	[88]
US/Fe <sub>3</sub> O <sub>4</sub> @MOF-2	200 W L <sup>-1</sup>	Diazinon	30 mg/L	0.7 g/L	PS	10 mM	120	98	Not mentioned	Commercially available	[128]
Fe <sup>0</sup> /US	40 kHz	Carbamazepine	1.0 mg L <sup>-1</sup>	0.4 g L <sup>-1</sup>	PDS	0.4 g L <sup>-1</sup>	60	98.4	Not mentioned	Commercially available	[37]

Tmp<sub>FG</sub>: a triphenylmethane derivative; SD: sulfadiazine; SMT: sulfamethazine. @: the composite of two materials.

### 4.3. Summary

The coupling activation of two iron-based catalysts under auxiliary action was introduced above. Both methods can accelerate the activation effect of iron-based catalysts on activation persulfate to a certain extent.

At present, the problem of photocatalysis is how to strengthen the application range of the photocatalyst. The treatment of industrial wastewater is generally conducted outdoors under complicated conditions. Some single photocatalysts, such as few-layered graphite-modified graphitic carbon nitride composite (GrCN), can be used in the degradation process together with PMS and photothermal catalysis [129]. The maximum reaction rate is  $0.044 \text{ min}^{-1}$ . The light source used for the data given in Table 5 is ultraviolet light, although sunlight contains only 5–7% of the ultraviolet spectrum. Therefore, how to improve the practicability of materials in the visible light range has become a new research direction.

Furthermore, if GrCN is used alone to degrade wastewater, not to mention the effect, recycling becomes a large problem. Therefore, it is a better method to compound it with a magnetic carrier. By combining magnetic iron oxide nanoparticles with the carrier, not only can the excellent catalytic effect of iron oxide be brought into play, but it can also facilitate the recovery of GrCN as a carrier, so that the two substances complement each other [130].

Piezoelectric catalysis, as a newly developed technology in recent years, still has a great space for development. Through ultrasonic and other methods that can generate vibration, oxidants and catalysts can be evenly dispersed into sewage to increase the contact point of chemical reaction, and more electrons can be generated by promoting piezoelectric materials to increase the concentration of free radicals and accelerate the progress of chemical reaction.

Table 7 shows the advantages and disadvantages of representative five iron-base catalysts mentioned above.

**Table 7.** Advantages and disadvantages of representative five iron-base catalysts mentioned above.

Catalyst	Advantages	Disadvantages	Ref.
CoFe <sub>2</sub> O <sub>4</sub>	CoFe <sub>2</sub> O <sub>4</sub> exhibited an excellent performance for ATZ removal (over 99%).	It has a good effect in activating PMS, but in activating PS and H <sub>2</sub> O <sub>2</sub> ; its recycling rate is not good due to the leaching of metal ions and loss of active sites.	[53]
CuFe <sub>2</sub> O <sub>4</sub> -20%rGO	Increase of specific surface area and chemical reaction activation sites.	The most suitable pH is 6.5; the application is limited.	[64]
Fe <sup>0</sup> @Fe <sub>3</sub> O <sub>4</sub>	It has high reactivity for atrazine degradation (near 100% removal in 2 min) and is highly stable in air.	The synthetic route is complex. It has a low stoichiometric efficiency (10.3%) because most PMS are ineffectively consumed during activation.	[90]
UV/Fe <sup>2+</sup>	Under the action of UV light, it shows an improved regeneration of Fe <sup>2+</sup> , causing a fast generation of highly reactive ·SO <sub>4</sub> <sup>-</sup> and ·OH.	Its applicable pH range is low (under 4). Too much catalyst will also reduce the reaction rate, so the use of catalyst needs to be strictly controlled.	[110]
US/ Fe <sup>0</sup>	The reaction rate was improved by coupling activation. Compared with pure catalyst, the degradation rate is also improved.	It is easily affected by the action of other anions in the solution (Cl <sup>-</sup> , NO <sub>3</sub> <sup>-</sup> ). Moreover, the effect of PMS alone is not good, and additional H <sub>2</sub> O <sub>2</sub> is needed to better degrade pollutants.	[125]

@: the composite of two materials.

## 5. Conclusions and Prospect

Activation persulfate technology based on iron-based catalysts has attracted wide attention in recent years. As for iron-based catalysts themselves because the central atom is Fe, their electron configuration is not in a full or partially full state, so their chemical properties are relatively active, and they are susceptible to not only pH but also various ions in water. SR-AOPs-PMS/PDS technology is new, and several metal ions mentioned above can activate persulfate. In terms of the current problems, several ideas and possibilities for improvement are proposed:

Adopt the multimetal composite method in the advanced oxidation technology of bimetal coordination. Taking iron as the core, screen and compare other metal ions of transition elements, and compound new iron-based catalyst.

Based on the data above, it is not difficult to see that the AOPs technology of nonfree radicals also has ideal effects. Compared with the generation of  $\cdot\text{SO}_4^-$ , the degradation effect of  $^1\text{O}_2$  produced by nonfree radicals is better to find a new nonfree radical reaction pathway to degrade wastewater.

After the reaction stops, the solubility of some iron-based catalysts or metal leaching may produce iron slag and other wastes. If the subsequent treatment is improper, it is easy to cause secondary pollution to the water body; at the same time, there is metal valency reaction in the reaction process, which reduces the collision of effective molecules and has more side reactions. How to improve the effective ion concentration for the reaction has become an urgent problem to be solved.

The persulfate used in the reaction is strongly oxidizing. If stored improperly or used in excess, it will produce a large toxic effect on organisms.

Most of the iron-based catalyst reaction conditions are acidic and create a strong acid environment. It is not applicable in a neutral environment. If used for degraded wastewater, the pH of water needs to be adjusted, and if there is acid intolerance or acid decomposition substances in the water, then it is easy to produce adverse consequences. Furthermore, the pH of water should be adjusted after the reaction is terminated, which greatly increases the cost.

Coupled catalysis based on iron-based catalysts with auxiliary action has played a good role in activation persulfate, and it is worthy of further study to improve the degradation effect by applying additional conditions. We can try to improve the performance of the materials with poor degradation effect among the 12 different iron-based catalysts mentioned above by photocatalysis, piezoelectric catalysis, and other methods.

Piezoelectric catalysis, as a research hotspot in recent years, is in its infancy at present. More kinds of catalysts can be produced by attempting to combine other transition metals and oxides with iron-based materials.

**Author Contributions:** Conceptualization, K.Z. and Z.L.; methodology, P.M.; software, Z.L. and P.M.; validation, Z.L., P.M., W.Z. and Y.T.; formal analysis, K.Z.; investigation, Y.Z. and W.Z.; resources, K.Z.; data curation, P.M.; writing—original draft preparation, Z.L. and J.Z.; writing—review and editing, Z.L.; visualization, Z.L.; supervision, K.Z.; project administration, K.Z.; funding acquisition, K.Z. All authors have read and agreed to the published version of the manuscript.

**Funding:** This review was funded by the Research Foundation of China University of Petroleum–Beijing at Karamay (grant number: YJ2018B02002).

**Acknowledgments:** This work was financially support by the Research Foundation of China University of Petroleum–Beijing at Karamay (grant number: YJ2018B02002). Thanks to the reviewers and editors for their valuable comments. I would like to express my heartfelt thanks to every author of the research group who actively participated in the work.

**Conflicts of Interest:** The authors declare no conflict of interest.

## References

1. Wang, G.; Bi, W.; Zhang, Q.; Dong, X.; Zhang, X. Hydrothermal carbonation carbon-based photocatalysis under visible light: Modification for enhanced removal of organic pollutant and novel insight into the photocatalytic mechanism. *J. Hazard. Mater.* **2021**, 127821. [[CrossRef](#)]
2. Van Gijn, K.; Chen, Y.L.; van Oudheusden, B.; Gong, S.; de Wilt, H.A.; Rijnaarts, H.H.M.; Langenhoff, A.A.M. Optimizing biological effluent organic matter removal for subsequent micropollutant removal. *J. Environ. Chem. Eng.* **2021**, *9*, 106247. [[CrossRef](#)]
3. Zeng, H.; Lan, H.; An, X.; Repo, E.; Park, Y.; Pastushok, O.; Liu, H.; Qu, J. Insight into electroreductive activation process of peroxydisulfate for eliminating organic pollution: Essential role of atomic hydrogen. *Chem. Eng. J.* **2021**, *426*, 128355. [[CrossRef](#)]
4. Giannakis, S.; Samoili, S.; Rodríguez-Chueca, J. A meta-analysis of the scientific literature on (photo)Fenton and persulfate advanced oxidation processes: Where do we stand and where are we heading to? *Curr. Opin. Green Sustain. Chem.* **2021**, *29*, 100456. [[CrossRef](#)]
5. Tian, Y.; Jia, N.; Zhou, L.; Lei, J.; Wang, L.; Zhang, J.; Liu, Y. Photo-Fenton-like degradation of antibiotics by inverse opal WO<sub>3</sub> co-catalytic Fe<sup>2+</sup>/PMS, Fe<sup>2+</sup>/H<sub>2</sub>O<sub>2</sub> and Fe<sup>2+</sup>/PDS processes: A comparative study. *Chemosphere* **2021**, 132627. [[CrossRef](#)]
6. Sathe, S.M.; Chakraborty, I.; Dubey, B.K.; Ghangrekar, M.M. Microbial fuel cell coupled Fenton oxidation for the cathodic degradation of emerging contaminants from wastewater: Applications and challenges. *Environ. Res.* **2022**, *204*, 112135. [[CrossRef](#)] [[PubMed](#)]
7. Mojiri, A.; Vakili, M.; Farraji, H.; Aziz, S.Q. Combined ozone oxidation process and adsorption methods for the removal of acetaminophen and amoxicillin from aqueous solution; kinetic and optimisation. *Environ. Technol. Innov.* **2019**, *15*, 100404. [[CrossRef](#)]
8. Zhu, B.; Jiang, G.; Chen, S.; Liu, F.; Wang, Y.; Zhao, C. Multifunctional Cl-S double-doped carbon nitride nanotube unit in catalytic ozone oxidation synergistic photocatalytic system: Generation of ROS-rich region and effective treatment of organic wastewater. *Chem. Eng. J.* **2022**, *430*, 132843. [[CrossRef](#)]
9. Tozar, T.; Boni, M.; Staicu, A.; Pascu, M.L. Optical Characterization of Ciprofloxacin Photolytic Degradation by UV-Pulsed Laser Radiation. *Molecules* **2021**, *26*, 2324. [[CrossRef](#)] [[PubMed](#)]
10. Mahbub, P.; Smallridge, A.; Irtassam, A.; Yeager, T. Scalable production of hydroxyl radicals (.OH) via homogeneous photolysis of hydrogen peroxide using a continuous-flow photoreactor. *Chem. Eng. J.* **2022**, *427*, 131762. [[CrossRef](#)]
11. Hsieh, M.-C.; Lai, W.W.-P.; Lin, A.Y.-C. Sunlight photolysis mitigates the formation of N-nitrosodimethylamine (NDMA) during the chloramination of methadone. *Chem. Eng. J.* **2020**, *384*, 123307. [[CrossRef](#)]
12. Ahmadpour, N.; Sayadi, M.H.; Sobhani, S.; Hajiani, M. A potential natural solar light active photocatalyst using magnetic ZnFe<sub>2</sub>O<sub>4</sub> @ TiO<sub>2</sub>/Cu nanocomposite as a high performance and recyclable platform for degradation of naproxen from aqueous solution. *J. Clean. Prod.* **2020**, *268*, 122023. [[CrossRef](#)]
13. Yin, R.; Chen, Y.; Hu, J.; Jin, S.; Guo, W.; Zhu, M. Peroxydisulfate bridged photocatalysis of covalent triazine framework for carbamazepine degradation. *Chem. Eng. J.* **2022**, *427*, 131613. [[CrossRef](#)]
14. Tang, P.; Liu, B.; Xie, W.; Wang, P.; He, Q.; Bao, J.; Zhang, Y.; Zhang, Z.; Li, J.; Ma, J. Synergistic mechanism of combined ferrate and ultrafiltration process for shale gas wastewater treatment. *J. Membr. Sci.* **2022**, *641*, 119921. [[CrossRef](#)]
15. Manoli, K.; Li, R.; Kim, J.; Feng, M.; Huang, C.-H.; Sharma, V.K. Ferrate(VI)-peracetic acid oxidation process: Rapid degradation of pharmaceuticals in water. *Chem. Eng. J.* **2022**, *429*, 132384. [[CrossRef](#)]
16. Pan, B.; Feng, M.; Qin, J.; Dar, A.A.; Wang, C.; Ma, X.; Sharma, V.K. Iron(V)/Iron(IV) species in graphitic carbon nitride-ferrate(VI)-visible light system: Enhanced oxidation of micropollutants. *Chem. Eng. J.* **2022**, *428*, 132610. [[CrossRef](#)]
17. Prasannamedha, G.; Kumar, P.S. A review on contamination and removal of sulfamethoxazole from aqueous solution using cleaner techniques: Present and future perspective. *J. Clean. Prod.* **2020**, *250*, 119553. [[CrossRef](#)]
18. Babu, D.S.; Srivastava, V.; Nidheesh, P.V.; Kumar, M.S. Detoxification of water and wastewater by advanced oxidation processes. *Sci. Total Environ.* **2019**, *696*, 133961. [[CrossRef](#)]
19. Hu, J.; Li, X.; Liu, F.; Fu, W.; Lin, L.; Li, B. Comparison of chemical and biological degradation of sulfonamides: Solving the mystery of sulfonamide transformation. *J. Hazard. Mater.* **2021**, 127661. [[CrossRef](#)]
20. Shimizu, A.; Takada, H.; Koike, T.; Takeshita, A.; Saha, M.; Rinawati; Nakada, N.; Murata, A.; Suzuki, T.; Suzuki, T.; et al. Ubiquitous occurrence of sulfonamides in tropical Asian waters. *Sci. Total Environ.* **2013**, *452–453*, 108–115. [[CrossRef](#)] [[PubMed](#)]
21. Chen, K.; Zhou, J.L. Occurrence and behavior of antibiotics in water and sediments from the Huangpu River, Shanghai, China. *Chemosphere* **2014**, *95*, 604–612. [[CrossRef](#)]
22. Li, Y.; Zhu, W.; Guo, Q.; Wang, X.; Zhang, L.; Gao, X.; Luo, Y. Highly efficient degradation of sulfamethoxazole (SMX) by activating peroxymonosulfate (PMS) with CoFe<sub>2</sub>O<sub>4</sub> in a wide pH range. *Sep. Purif. Technol.* **2021**, *276*, 119403. [[CrossRef](#)]
23. Wang, S.; Wang, J. Synergistic effect of PMS activation by Fe<sup>0</sup>@Fe<sub>3</sub>O<sub>4</sub> anchored on N, S, O co-doped carbon composite for degradation of sulfamethoxazole. *Chem. Eng. J.* **2022**, *427*, 131960. [[CrossRef](#)]
24. Zhang, T.; Liu, Y.; Zhong, S.; Zhang, L. AOPs-based remediation of petroleum hydrocarbons-contaminated soils: Efficiency, influencing factors and environmental impacts. *Chemosphere* **2019**, *246*, 125726. [[CrossRef](#)]
25. Zhang, J.; Song, H.; Liu, Y.; Wang, L.; Li, D.; Liu, C.; Gong, M.; Zhang, Z.; Yang, T.; Ma, J. Remarkable enhancement of a photochemical Fenton-like system (UV-A/Fe(II)/PMS) at near-neutral pH and low Fe(II)/peroxymonosulfate ratio by three alpha hydroxy acids: Mechanisms and influencing factors. *Sep. Purif. Technol.* **2019**, *224*, 142–151. [[CrossRef](#)]

26. Yang, L.; He, L.; Xue, J.; Ma, Y.; Xie, Z.; Wu, L.; Huang, M.; Zhang, Z. Persulfate-based degradation of perfluorooctanoic acid (PFOA) and perfluorooctane sulfonate (PFOS) in aqueous solution: Review on influences, mechanisms and prospective. *J. Hazard. Mater.* **2020**, *393*, 122405. [[CrossRef](#)] [[PubMed](#)]
27. Ding, R.-R.; Li, W.-Q.; He, C.-S.; Wang, Y.-R.; Liu, X.-C.; Zhou, G.-N.; Mu, Y. Oxygen vacancy on hollow sphere  $\text{CuFe}_2\text{O}_4$  as an efficient Fenton-like catalysis for organic pollutant degradation over a wide pH range. *Appl. Catal. B Environ.* **2021**, *291*, 120069. [[CrossRef](#)]
28. Liu, F.; Zhang, Y.; Wang, S.; Gong, T.; Hua, M.; Qian, J.; Pan, B. Metal-free biomass with abundant carbonyl groups as efficient catalyst for the activation of peroxymonosulfate and degradation of sulfamethoxazole. *Chem. Eng. J.* **2022**, *430*, 132767. [[CrossRef](#)]
29. Zhang, W.; Qian, L.; Han, L.; Yang, L.; Ouyang, D.; Long, Y.; Wei, Z.; Dong, X.; Liang, C.; Li, J.; et al. Synergistic roles of Fe(II) on simultaneous removal of hexavalent chromium and trichloroethylene by attapulgite-supported nanoscale zero-valent iron/persulfate system. *Chem. Eng. J.* **2022**, *430*, 132841. [[CrossRef](#)]
30. Keerthana, S.P.; Yuvakkumar, R.; Ravi, G.; Pavithra, S.; Thambidurai, M.; Dang, C.; Velauthapillai, D. Pure and Ce-doped spinel  $\text{CuFe}_2\text{O}_4$  photocatalysts for efficient rhodamine B degradation. *Environ. Res.* **2021**, *200*, 111528. [[CrossRef](#)]
31. Wu, R.; Qu, J.; He, H.; Yu, Y. Removal of azo-dye Acid Red B (ARB) by adsorption and catalytic combustion using magnetic  $\text{CuFe}_2\text{O}_4$  powder. *Appl. Catal. B Environ.* **2004**, *48*, 49–56. [[CrossRef](#)]
32. Ding, Y.; Zhu, L.; Wang, N.; Tang, H. Sulfate radicals induced degradation of tetrabromobisphenol A with nanoscaled magnetic  $\text{CuFe}_2\text{O}_4$  as a heterogeneous catalyst of peroxymonosulfate. *Appl. Catal. B Environ.* **2013**, *129*, 153–162. [[CrossRef](#)]
33. Salami, R.; Amini, M.; Bagherzadeh, M.; Chae, K.H. Vanadium oxide-supported copper ferrite nanoparticles: A reusable and highly efficient catalyst for rhodamine B degradation via activation of peroxymonosulfate. *Appl. Organomet. Chem.* **2021**, *35*. [[CrossRef](#)]
34. Yi, X.-H.; Ji, H.; Wang, C.-C.; Li, Y.; Li, Y.-H.; Zhao, C.; Wang, A.; Fu, H.; Wang, P.; Zhao, X.; et al. Photocatalysis-activated SR-AOP over PDINH/MIL-88A(Fe) composites for boosted chloroquine phosphate degradation: Performance, mechanism, pathway and DFT calculations. *Appl. Catal. B Environ.* **2021**, *293*, 120229. [[CrossRef](#)]
35. Duan, P.; Liu, X.; Liu, B.; Akram, M.; Li, Y.; Pan, J.; Yue, Q.; Gao, B.; Xu, X. Effect of phosphate on peroxymonosulfate activation: Accelerating generation of sulfate radical and underlying mechanism. *Appl. Catal. B Environ.* **2021**, *298*, 120532. [[CrossRef](#)]
36. Fan, X.; Wang, Y.; Zhang, D.; Guo, Y.; Gao, S.; Li, E.; Zheng, H. Effects of acid, acid-ZVI/PMS, Fe(II)/PMS and ZVI/PMS conditioning on the wastewater activated sludge (WAS) dewaterability and extracellular polymeric substances (EPS). *J. Environ. Sci.* **2020**, *91*, 73–84. [[CrossRef](#)]
37. Wei, W.; Zhou, D.; Feng, L.; Li, X.; Hu, L.; Zheng, H.; Wang, Y. The graceful art, significant function and wide application behavior of ultrasound research and understanding in carbamazepine (CBZ) enhanced removal and degradation by FeO/PDS/US. *Chemosphere* **2021**, *278*, 130368. [[CrossRef](#)]
38. Wang, J.; Wang, S. Activation of persulfate (PS) and peroxymonosulfate (PMS) and application for the degradation of emerging contaminants. *Chem. Eng. J.* **2018**, *334*, 1502–1517. [[CrossRef](#)]
39. Li, Y.; Ma, S.; Xu, S.; Fu, H.; Li, Z.; Li, K.; Sheng, K.; Du, J.; Lu, X.; Li, X.; et al. Novel magnetic biochar as an activator for peroxymonosulfate to degrade bisphenol A: Emphasizing the synergistic effect between graphitized structure and  $\text{CoFe}_2\text{O}_4$ . *Chem. Eng. J.* **2020**, *387*, 124094. [[CrossRef](#)]
40. Wang, X.; Wang, A.; Ma, J. Visible-light-driven photocatalytic removal of antibiotics by newly designed  $\text{C}_3\text{N}_4@\text{MnFe}_2\text{O}_4$ -graphene nanocomposites. *J. Hazard. Mater.* **2017**, *336*, 81–92. [[CrossRef](#)]
41. Huang, Y.; Han, C.; Liu, Y.; Nadagouda, M.N.; Machala, L.; O'Shea, K.E.; Sharma, V.K.; Dionysiou, D.D. Degradation of atrazine by  $\text{ZnxCu}_{1-x}\text{Fe}_2\text{O}_4$  nanomaterial-catalyzed sulfite under UV-vis light irradiation: Green strategy to generate  $\text{SO}_4^{\cdot-}$ . *Appl. Catal. B Environ.* **2018**, *221*, 380–392. [[CrossRef](#)]
42. Jaafarzadeh, N.; Ghanbari, F.; Ahmadi, M. Efficient degradation of 2,4-dichlorophenoxyacetic acid by peroxymonosulfate/magnetic copper ferrite nanoparticles/ozone: A novel combination of advanced oxidation processes. *Chem. Eng. J.* **2017**, *320*, 436–447. [[CrossRef](#)]
43. Song, Y.; Yang, Y.; Mo, S.; Guo, D.; Liu, L. Fast construction of  $(\text{Fe}_2\text{O}_3)_x@\text{Ni-MOF}$  heterostructure nanosheets as highly active catalyst for water oxidation. *J. Alloys Compd.* **2022**, *892*, 162149. [[CrossRef](#)]
44. Lyu, L.; Won Kim, C.; Seong, K.-D.; Kang, J.; Liu, S.; Yamauchi, Y.; Piao, Y. Defect engineering induced heterostructure of Zn-birnessite@spinel  $\text{ZnMn}_2\text{O}_4$  nanocrystal for flexible asymmetric supercapacitor. *Chem. Eng. J.* **2021**, 133115. [[CrossRef](#)]
45. Xie, X.; Wang, B.; Wang, Y.; Ni, C.; Sun, X.; Du, W. Spinel structured  $\text{MFe}_2\text{O}_4$  (M = Fe, Co, Ni, Mn, Zn) and their composites for microwave absorption: A review. *Chem. Eng. J.* **2022**, *428*, 131160. [[CrossRef](#)]
46. Xian, G.; Kong, S.; Li, Q.; Zhang, G.; Zhou, N.; Du, H.; Niu, L. Synthesis of Spinel Ferrite  $\text{MFe}_2\text{O}_4$  (M = Co, Cu, Mn, and Zn) for Persulfate Activation to Remove Aqueous Organics: Effects of M-Site Metal and Synthetic Method. *Front. Chem.* **2020**, *8*. [[CrossRef](#)]
47. Yang, Z.; Li, Y.; Zhang, X.; Cui, X.; He, S.; Liang, H.; Ding, A. Sludge activated carbon-based  $\text{CoFe}_2\text{O}_4$ -SAC nanocomposites used as heterogeneous catalysts for degrading antibiotic norfloxacin through activating peroxymonosulfate. *Chem. Eng. J.* **2020**, *384*, 123319. [[CrossRef](#)]
48. Mostafa, S.; Rosario-Ortiz, F.L. Singlet oxygen formation from wastewater organic matter. *Environ. Sci. Technol.* **2013**, *47*, 8179–8186. [[CrossRef](#)]

49. Yi, Q.; Ji, J.; Shen, B.; Dong, C.; Liu, J.; Zhang, J.; Xing, M. Singlet Oxygen Triggered by Superoxide Radicals in a Molybdenum Cocatalytic Fenton Reaction with Enhanced REDOX Activity in the Environment. *Environ. Sci. Technol.* **2019**, *53*, 9725–9733. [[CrossRef](#)]
50. Mikrut, M.; Mazuryk, O.; Macyk, W.; van Eldik, R.; Stochel, G. Generation and photogeneration of hydroxyl radicals and singlet oxygen by particulate matter and its inorganic components. *J. Environ. Chem. Eng.* **2021**, *9*, 106478. [[CrossRef](#)]
51. Liu, F.; Li, W.; Wu, D.; Tian, T.; Wu, J.-F.; Dong, Z.-M.; Zhao, G.-C. New insight into the mechanism of peroxymonosulfate activation by nanoscaled lead-based spinel for organic matters degradation: A singlet oxygen-dominated oxidation process. *J. Colloid Interface Sci.* **2020**, *572*, 318–327. [[CrossRef](#)] [[PubMed](#)]
52. Gao, D.; Junaid, M.; Lin, F.; Zhang, S.; Xu, N. Degradation of sulphachloropyridazine sodium in column reactor packed with  $\text{CoFe}_2\text{O}_4$ -loaded quartz sand via peroxymonosulfate activation: Insights into the amorphous phase, efficiency, and mechanism. *Chem. Eng. J.* **2020**, *390*, 124549. [[CrossRef](#)]
53. Li, J.; Xu, M.; Yao, G.; Lai, B. Enhancement of the degradation of atrazine through  $\text{CoFe}_2\text{O}_4$  activated peroxymonosulfate (PMS) process: Kinetic, degradation intermediates, and toxicity evaluation. *Chem. Eng. J.* **2018**, *348*, 1012–1024. [[CrossRef](#)]
54. Ratanaphain, C.; Viboonratanasri, D.; Prompinit, P.; Krajangpan, S.; Khan, E.; Punyapalakul, P. Reactivity characterization of  $\text{SiO}_2$ -coated nano zero-valent iron for iodoacetamide degradation: The effects of  $\text{SiO}_2$  thickness, and the roles of dehalogenation, hydrolysis and adsorption. *Chemosphere* **2022**, *286*, 131816. [[CrossRef](#)] [[PubMed](#)]
55. Ding, S.; Wan, J.; Wang, Y.; Yan, Z.; Ma, Y. Activation of persulfate by molecularly imprinted Fe-MOF-74@ $\text{SiO}_2$  for the targeted degradation of dimethyl phthalate: Effects of operating parameters and chlorine. *Chem. Eng. J.* **2021**, *422*, 130406. [[CrossRef](#)]
56. Wang, L.; Guan, R.; Qi, Y.; Zhang, F.; Li, P.; Wang, J.; Qu, P.; Zhou, G.; Shi, W. Constructing Zn-P charge transfer bridge over  $\text{ZnFe}_2\text{O}_4$ -black phosphorus 3D microcavity structure: Efficient photocatalyst design in visible-near-infrared region. *J. Colloid Interface Sci.* **2021**, *600*, 463–472. [[CrossRef](#)]
57. Shao, S.; Deng, J.; Lv, X.; Ji, H.; Xiao, Y.; Zhu, X.; Feng, K.; Xu, H.; Zhong, J. Black phosphorus nanoflakes decorated hematite photoanode with functional phosphate bridges for enhanced water oxidation. *Chem. Eng. J.* **2021**, *425*, 131500. [[CrossRef](#)]
58. Askari, M.B.; Salarizadeh, P.; Beitollahi, H.; Tajik, S.; Eshghi, A.; Azizi, S. Electro-oxidation of hydrazine on  $\text{NiFe}_2\text{O}_4$ -rGO as a high-performance nano-electrocatalyst in alkaline media. *Mater. Chem. Phys.* **2022**, *275*, 125313. [[CrossRef](#)]
59. Wang, X.; Wang, D.; Ma, C.; Yang, Z.; Yue, H.; Zhang, D.; Sun, Z. Conductive  $\text{Fe}_2\text{N}/\text{N-rGO}$  composite boosts electrochemical redox reactions in wide temperature accommodating lithium-sulfur batteries. *Chem. Eng. J.* **2022**, *427*, 131622. [[CrossRef](#)]
60. Karthikeyan, C.; Ramachandran, K.; Sheet, S.; Yoo, D.J.; Lee, Y.S.; Satish kumar, Y.; Kim, A.R.; Gnana kumar, G. Pigeon-Excreta-Mediated Synthesis of Reduced Graphene Oxide (rGO)/ $\text{CuFe}_2\text{O}_4$  Nanocomposite and Its Catalytic Activity toward Sensitive and Selective Hydrogen Peroxide Detection. *ACS Sustain. Chem. Eng.* **2017**, *5*, 4897–4905. [[CrossRef](#)]
61. Othman, I.; Abu Haija, M.; Ismail, I.; Zain, J.H.; Banat, F. Preparation and catalytic performance of  $\text{CuFe}_2\text{O}_4$  nanoparticles supported on reduced graphene oxide ( $\text{CuFe}_2\text{O}_4/\text{rGO}$ ) for phenol degradation. *Mater. Chem. Phys.* **2019**, *238*. [[CrossRef](#)]
62. Wang, W.; Yu, J.C.; Xia, D.; Wong, P.K.; Li, Y. Graphene and g- $\text{C}_3\text{N}_4$  nanosheets cowrapped elemental alpha-sulfur as a novel metal-free heterojunction photocatalyst for bacterial inactivation under visible-light. *Environ. Sci. Technol.* **2013**, *47*, 8724–8732. [[CrossRef](#)]
63. Sun, B.; Ma, W.; Wang, N.; Xu, P.; Zhang, L.; Wang, B.; Zhao, H.; Lin, K.A.; Du, Y. Retraction of “Polyaniline: A New Metal-Free Catalyst for Peroxymonosulfate Activation with Highly Efficient and Durable Removal of Organic Pollutants”. *Environ. Sci. Technol.* **2021**, *55*, 3451. [[CrossRef](#)]
64. Hao, P.; Hu, M.; Xing, R.; Zhou, W. Synergistic degradation of methylparaben on  $\text{CuFe}_2\text{O}_4$ -rGO composite by persulfate activation. *J. Alloys Compd.* **2020**, *823*, 153757. [[CrossRef](#)]
65. Li, R.; Cai, M.; Xie, Z.; Zhang, Q.; Zeng, Y.; Liu, H.; Liu, G.; Lv, W. Construction of heterostructured  $\text{CuFe}_2\text{O}_4/\text{g-C}_3\text{N}_4$  nanocomposite as an efficient visible light photocatalyst with peroxydisulfate for the organic oxidation. *Appl. Catal. B Environ.* **2019**, *244*, 974–982. [[CrossRef](#)]
66. Gan, L.; Zhong, Q.; Geng, A.; Wang, L.; Song, C.; Han, S.; Cui, J.; Xu, L. Cellulose derived carbon nanofiber: A promising biochar support to enhance the catalytic performance of  $\text{CoFe}_2\text{O}_4$  in activating peroxymonosulfate for recycled dimethyl phthalate degradation. *Sci. Total Environ.* **2019**, *694*, 133705. [[CrossRef](#)]
67. Golshan, M.; Kakavandi, B.; Ahmadi, M.; Azizi, M. Photocatalytic activation of peroxymonosulfate by  $\text{TiO}_2$  anchored on copper ferrite ( $\text{TiO}_2@/\text{CuFe}_2\text{O}_4$ ) into 2,4-D degradation: Process feasibility, mechanism and pathway. *J. Hazard. Mater.* **2018**, *359*, 325–337. [[CrossRef](#)]
68. Zhu, B.; Cheng, H.; Ma, J.; Kong, Y.; Komarneni, S. Efficient degradation of rhodamine B by magnetically separable ZnS-Zn $\text{Fe}_2\text{O}_4$  composite with the synergistic effect from persulfate. *Chemosphere* **2019**, *237*, 124547. [[CrossRef](#)] [[PubMed](#)]
69. Kohantorabi, M.; Hosseini-fard, M.; Kazemzadeh, A. Catalytic activity of a magnetic  $\text{Fe}_2\text{O}_3@/\text{CoFe}_2\text{O}_4$  nanocomposite in peroxy-monosulfate activation for norfloxacin removal. *N. J. Chem.* **2020**, *44*, 4185–4198. [[CrossRef](#)]
70. Zhang, X.; Feng, M.; Wang, L.; Qu, R.; Wang, Z. Catalytic degradation of 2-phenylbenzimidazole-5-sulfonic acid by peroxy-monosulfate activated with nitrogen and sulfur co-doped CNTs-COOH loaded  $\text{CuFe}_2\text{O}_4$ . *Chem. Eng. J.* **2017**, *307*, 95–104. [[CrossRef](#)]
71. Cuervo Lumbaque, E.; Lopes Tiburtius, E.R.; Barreto-Rodrigues, M.; Sirtori, C. Current trends in the use of zero-valent iron ( $\text{Fe}^0$ ) for degradation of pharmaceuticals present in different water matrices. *Trends Environ. Anal. Chem.* **2019**, *24*, e00069. [[CrossRef](#)]

72. Hussain, I.; Zhang, Y.; Huang, S.; Gao, Q. Degradation of p-chloroaniline by  $\text{FeO}_3-x\text{H}_3-2x/\text{Fe}^0$  in the presence of persulfate in aqueous solution. *RSC Adv.* **2015**, *5*, 41079–41087. [CrossRef]
73. Rodriguez, S.; Vasquez, L.; Romero, A.; Santos, A. Dye Oxidation in Aqueous Phase by Using Zero-Valent Iron as Persulfate Activator: Kinetic Model and Effect of Particle Size. *Ind. Eng. Chem. Res.* **2014**, *53*, 12288–12294. [CrossRef]
74. Li, J.; Zhang, X.; Sun, Y.; Liang, L.; Pan, B.; Zhang, W.; Guan, X. Advances in Sulfidation of Zerovalent Iron for Water Decontamination. *Environ. Sci. Technol.* **2017**, *51*, 13533–13544. [CrossRef] [PubMed]
75. Xiao, S.; Cheng, M.; Zhong, H.; Liu, Z.; Liu, Y.; Yang, X.; Liang, Q. Iron-mediated activation of persulfate and peroxymonosulfate in both homogeneous and heterogeneous ways: A review. *Chem. Eng. J.* **2020**, *384*, 123265. [CrossRef]
76. Wang, Z.; Qiu, W.; Pang, S.-Y.; Zhou, Y.; Gao, Y.; Guan, C.; Jiang, J. Further understanding the involvement of Fe(IV) in peroxydisulfate and peroxymonosulfate activation by Fe(II) for oxidative water treatment. *Chem. Eng. J.* **2019**, *371*, 842–847. [CrossRef]
77. Huang, J.; Zhang, H. Mn-based catalysts for sulfate radical-based advanced oxidation processes: A review. *Environ. Int.* **2019**, *133*, 105141. [CrossRef]
78. Zheng, X.; Niu, X.; Zhang, D.; Lv, M.; Ye, X.; Ma, J.; Lin, Z.; Fu, M. Metal-based catalysts for persulfate and peroxymonosulfate activation in heterogeneous ways: A review. *Chem. Eng. J.* **2022**, *429*, 132323. [CrossRef]
79. Weng, C.H.; Ding, F.; Lin, Y.T.; Liu, N. Effective decolorization of polyazo direct dye Sirius Red F3B using persulfate activated with Fe-0 aggregate. *Sep. Purif. Technol.* **2015**, *147*, 147–155. [CrossRef]
80. Li, H.; Wan, J.; Ma, Y.; Wang, Y.; Huang, M. Influence of particle size of zero-valent iron and dissolved silica on the reactivity of activated persulfate for degradation of acid orange 7. *Chem. Eng. J.* **2014**, *237*, 487–496. [CrossRef]
81. Wang, Z.; Qiu, W.; Pang, S.; Gao, Y.; Zhou, Y.; Cao, Y.; Jiang, J. Relative contribution of ferryl ion species (Fe(IV)) and sulfate radical formed in nanoscale zero valent iron activated peroxydisulfate and peroxymonosulfate processes. *Water Res.* **2020**, *172*, 115504. [CrossRef] [PubMed]
82. Li, X.; Zhou, M.; Pan, Y. Enhanced degradation of 2,4-dichlorophenoxyacetic acid by pre-magnetization Fe-C activated persulfate: Influential factors, mechanism and degradation pathway. *J. Hazard. Mater.* **2018**, *353*, 454–465. [CrossRef]
83. Ye, C.; Liu, P.; Ma, Z.; Xue, C.; Zhang, C.; Zhang, Y.; Liu, J.; Liu, C.; Sun, X.; Mu, Y. High  $\text{H}_2\text{O}_2$  Concentrations Observed during Haze Periods during the Winter in Beijing: Importance of  $\text{H}_2\text{O}_2$  Oxidation in Sulfate Formation. *Environ. Sci. Technol. Lett.* **2018**, *5*, 757–763. [CrossRef]
84. Peng, X.; Xi, B.; Zhao, Y.; Shi, Q.; Meng, X.; Mao, X.; Jiang, Y.; Ma, Z.; Tan, W.; Liu, H.; et al. Effect of Arsenic on the Formation and Adsorption Property of Ferric Hydroxide Precipitates in ZVI Treatment. *Environ. Sci. Technol.* **2017**, *51*, 10100–10108. [CrossRef]
85. Wu, J.; Wang, B.; Cagnetta, G.; Huang, J.; Wang, Y.; Deng, S.; Yu, G. Nanoscale zero valent iron-activated persulfate coupled with Fenton oxidation process for typical pharmaceuticals and personal care products degradation. *Sep. Purif. Technol.* **2020**, *239*, 116534. [CrossRef]
86. Zhang, T.; Yang, Y.; Gao, J.; Li, X.; Yu, H.; Wang, N.; Du, P.; Yu, R.; Li, H.; Fan, X.; et al. Synergistic degradation of chloramphenicol by ultrasound-enhanced nanoscale zero-valent iron/persulfate treatment. *Sep. Purif. Technol.* **2020**, *240*, 116575. [CrossRef]
87. Chen, L.; Huang, Y.; Zhou, M.; Xing, K.; Lv, W.; Wang, W.; Chen, H.; Yao, Y. Nitrogen-doped porous carbon encapsulating iron nanoparticles for enhanced sulfathiazole removal via peroxymonosulfate activation. *Chemosphere* **2020**, *250*, 126300. [CrossRef] [PubMed]
88. Li, S.; Tang, J.; Liu, Q.; Liu, X.; Gao, B. A novel stabilized carbon-coated nZVI as heterogeneous persulfate catalyst for enhanced degradation of 4-chlorophenol. *Environ. Int.* **2020**, *138*, 105639. [CrossRef]
89. Li, H.; Wan, J.; Ma, Y.; Wang, Y. Synthesis of novel core-shell  $\text{Fe}^0/\text{Fe}_3\text{O}_4$  as heterogeneous activator of persulfate for oxidation of dibutyl phthalate under neutral conditions. *Chem. Eng. J.* **2016**, *301*, 315–324. [CrossRef]
90. Feng, Y.; Zhong, J.; Zhang, L.; Fan, Y.; Yang, Z.; Shih, K.; Li, H.; Wu, D.; Yan, B. Activation of peroxymonosulfate by  $\text{Fe}^0/\text{Fe}_3\text{O}_4$  core-shell nanowires for sulfate radical generation: Electron transfer and transformation products. *Sep. Purif. Technol.* **2020**, *247*, 116942. [CrossRef]
91. Liu, Y.; Guo, H.; Zhang, Y.; Cheng, X.; Zhou, P.; Wang, J.; Li, W. Fe@C carbonized resin for peroxymonosulfate activation and bisphenol S degradation. *Environ. Pollut.* **2019**, *252*, 1042–1050. [CrossRef] [PubMed]
92. Guo, F.; Wang, K.; Lu, J.; Chen, J.; Dong, X.; Xia, D.; Zhang, A.; Wang, Q. Activation of peroxymonosulfate by magnetic carbon supported Prussian blue nanocomposite for the degradation of organic contaminants with singlet oxygen and superoxide radicals. *Chemosphere* **2019**, *218*, 1071–1081. [CrossRef] [PubMed]
93. Wang, H.; Zhang, C.; Zhang, X.; Wang, S.; Xia, Z.; Zeng, G.; Ding, J.; Ren, N. Construction of  $\text{Fe}_3\text{O}_4/\beta\text{-CD}/\text{g-C}_3\text{N}_4$  nanocomposite catalyst for degradation of PCBs in wastewater through photodegradation and heterogeneous Fenton oxidation. *Chem. Eng. J.* **2022**, *429*, 132445. [CrossRef]
94. He, J.; Song, G.; Wang, X.; Zhou, L.; Li, J. Multifunctional magnetic  $\text{Fe}_3\text{O}_4/\text{GO}/\text{Ag}$  composite microspheres for SERS detection and catalytic degradation of methylene blue and ciprofloxacin. *J. Alloys Compd.* **2022**, *893*, 162226. [CrossRef]
95. Zhen, J.; Zhang, S.; Zhuang, X.; Ahmad, S.; Lee, T.; Si, H.; Cao, C.; Ni, S.-Q. Sulfate radicals based heterogeneous peroxymonosulfate system catalyzed by  $\text{CuO-Fe}_3\text{O}_4\text{-Biochar}$  nanocomposite for bisphenol A degradation. *J. Water Process Eng.* **2021**, *41*, 102078. [CrossRef]
96. Yin, F.; Wang, C.; Lin, K.-Y.A.; Tong, S. Persulfate activation for efficient degradation of norfloxacin by a rGO- $\text{Fe}_3\text{O}_4$  composite. *J. Taiwan Inst. Chem. Eng.* **2019**, *102*, 163–169. [CrossRef]

97. Yan, J.; Lei, M.; Zhu, L.; Anjum, M.N.; Zou, J.; Tang, H. Degradation of sulfamonomethoxine with Fe<sub>3</sub>O<sub>4</sub> magnetic nanoparticles as heterogeneous activator of persulfate. *J. Hazard. Mater.* **2011**, *186*, 1398–1404. [[CrossRef](#)] [[PubMed](#)]
98. Wu, Z.; Wang, Y.; Xiong, Z.; Ao, Z.; Pu, S.; Yao, G.; Lai, B. Core-shell magnetic Fe<sub>3</sub>O<sub>4</sub>@Zn/Co-ZIFs to activate peroxymonosulfate for highly efficient degradation of carbamazepine. *Appl. Catal. B Environ.* **2020**, *277*, 119136. [[CrossRef](#)]
99. Zhao, G.; Zou, J.; Chen, X.; Liu, L.; Wang, Y.; Zhou, S.; Long, X.; Yu, J.; Jiao, F. Iron-based catalysts for persulfate-based advanced oxidation process: Microstructure, property and tailoring. *Chem. Eng. J.* **2021**, *421*, 127845. [[CrossRef](#)]
100. Fu, H.; Zhao, P.; Xu, S.; Cheng, G.; Li, Z.; Li, Y.; Li, K.; Ma, S. Fabrication of Fe<sub>3</sub>O<sub>4</sub> and graphitized porous biochar composites for activating peroxymonosulfate to degrade p-hydroxybenzoic acid: Insights on the mechanism. *Chem. Eng. J.* **2019**, *375*, 121980. [[CrossRef](#)]
101. Lu, J.-D. The effect of two ferromagnetic metal stripes on valley polarization of electrons in a graphene. *Phys. Lett. A* **2020**, *384*, 126402. [[CrossRef](#)]
102. Brovini, E.M.; de Deus, B.C.T.; Vilas-Boas, J.A.; Quadra, G.R.; Carvalho, L.; Mendonça, R.F.; Pereira, R.D.O.; Cardoso, S.J. Three-best-selling pesticides in Brazil: Freshwater concentrations and potential environmental risks. *Sci. Total Environ.* **2021**, *771*, 144754. [[CrossRef](#)]
103. Wang, F.; Gao, J.; Zhai, W.; Cui, J.; Liu, D.; Zhou, Z.; Wang, P. Effects of antibiotic norfloxacin on the degradation and enantioselectivity of the herbicides in aquatic environment. *Ecotoxicol. Environ. Saf.* **2021**, *208*, 111717. [[CrossRef](#)] [[PubMed](#)]
104. Balakrishna, K.; Rath, A.; Praveenkumarreddy, Y.; Guruge, K.S.; Subedi, B. A review of the occurrence of pharmaceuticals and personal care products in Indian water bodies. *Ecotoxicol. Environ. Saf.* **2017**, *137*, 113–120. [[CrossRef](#)]
105. Harnett, K.G.; Chin, A.; Schuh, S.M. BPA and BPA alternatives BPS, BPAF, and TMBPF, induce cytotoxicity and apoptosis in rat and human stem cells. *Ecotoxicol. Environ. Saf.* **2021**, *216*, 112210. [[CrossRef](#)]
106. Yang, Q.; Ma, Y.; Chen, F.; Yao, F.; Sun, J.; Wang, S.; Yi, K.; Hou, L.; Li, X.; Wang, D. Recent advances in photo-activated sulfate radical-advanced oxidation process (SR-AOP) for refractory organic pollutants removal in water. *Chem. Eng. J.* **2019**, *378*, 122149. [[CrossRef](#)]
107. Khan, J.A.; He, X.; Khan, H.M.; Shah, N.S.; Dionysiou, D.D. Oxidative degradation of atrazine in aqueous solution by UV/H<sub>2</sub>O<sub>2</sub>/Fe<sup>2+</sup>, UV/S<sub>2</sub>O<sub>8</sub><sup>2-</sup>/Fe<sup>2+</sup> and UV/HSO<sub>5</sub><sup>-</sup>/Fe<sup>2+</sup> processes: A comparative study. *Chem. Eng. J.* **2013**, *218*, 376–383. [[CrossRef](#)]
108. Devi, L.G.; Munikrishnappa, C.; Nagaraj, B.; Rajashekhar, K.E. Effect of chloride and sulfate ions on the advanced photo Fenton and modified photo Fenton degradation process of Alizarin Red S. *J. Mol. Catal. A Chem.* **2013**, *374–375*, 125–131. [[CrossRef](#)]
109. Benkelberg, H.-J.; Warneck, P. Photodecomposition of Iron(III) Hydroxo and Sulfato Complexes in Aqueous Solution: Wavelength Dependence of OH and SO<sub>4</sub><sup>-</sup> Quantum Yields. *J. Phys. Chem.* **1995**, *99*, 5214–5221. [[CrossRef](#)]
110. Khan, S.; He, X.; Khan, H.M.; Boccelli, D.; Dionysiou, D.D. Efficient degradation of lindane in aqueous solution by iron (II) and/or UV activated peroxymonosulfate. *J. Photochem. Photobiol. A Chem.* **2016**, *316*, 37–43. [[CrossRef](#)]
111. Jaafarzadeh, N.; Ghanbari, F.; Ahmadi, M. Catalytic degradation of 2,4-dichlorophenoxyacetic acid (2,4-D) by nano-Fe<sub>2</sub>O<sub>3</sub> activated peroxymonosulfate: Influential factors and mechanism determination. *Chemosphere* **2017**, *169*, 568–576. [[CrossRef](#)] [[PubMed](#)]
112. Ahmed, M.M.; Chiron, S. Solar photo-Fenton like using persulphate for carbamazepine removal from domestic wastewater. *Water Res.* **2014**, *48*, 229–236. [[CrossRef](#)]
113. Ahmed, M.M.; Brienza, M.; Goetz, V.; Chiron, S. Solar photo-Fenton using peroxymonosulfate for organic micropollutants removal from domestic wastewater: Comparison with heterogeneous TiO<sub>2</sub> photocatalysis. *Chemosphere* **2014**, *117*, 256–261. [[CrossRef](#)] [[PubMed](#)]
114. Zhu, K.; Wang, J.; Wang, Y.; Jin, C.; Ganeshraja, A.S. Visible-light-induced photocatalysis and peroxymonosulfate activation over ZnFe<sub>2</sub>O<sub>4</sub> fine nanoparticles for degradation of Orange II. *Catal. Sci. Technol.* **2016**, *6*, 2296–2304. [[CrossRef](#)]
115. Cai, C.; Liu, J.; Zhang, Z.; Zheng, Y.; Zhang, H. Visible light enhanced heterogeneous photo-degradation of Orange II by zinc ferrite (ZnFe<sub>2</sub>O<sub>4</sub>) catalyst with the assistance of persulfate. *Sep. Purif. Technol.* **2016**, *165*, 42–52. [[CrossRef](#)]
116. Villa, S.M.; Maturi, M.; Santaniello, T.; Migliorini, L.; Locatelli, E.; Franchini, M.C.; Milani, P. Quantitative Spectral Electromechanical Characterization of Soft Piezoelectric Nanocomposites. *Sens. Actuators A Phys.* **2021**, 113196. [[CrossRef](#)]
117. Tan, D.; Jiang, C.; Sun, N.; Huang, J.; Zhang, Z.; Zhang, Q.; Bu, J.; Bi, S.; Guo, Q.; Song, J. Piezoelectricity in monolayer MXene for nanogenerators and piezotronics. *Nano Energy* **2021**, *90*, 106528. [[CrossRef](#)]
118. Wang, P.; Li, X.; Fan, S.; Chen, X.; Qin, M.; Long, D.; Tadé, M.O.; Liu, S. Impact of oxygen vacancy occupancy on piezo-catalytic activity of BaTiO<sub>3</sub> nanobelt. *Appl. Catal. B Environ.* **2020**, *279*, 119340. [[CrossRef](#)]
119. Yang, X.; Li, P.; Wu, B.; Li, H.; Zhou, G. A flexible piezoelectric-triboelectric hybrid nanogenerator in one structure with dual doping enhancement effects. *Curr. Appl. Phys.* **2021**, *32*, 50–58. [[CrossRef](#)]
120. Xu, Q.; Zhang, H.; Leng, H.; You, H.; Jia, Y.; Wang, S. Ultrasonic role to activate persulfate/chlorite with foamed zero-valent-iron: Sonochemical applications and induced mechanisms. *Ultrason. Sonochem.* **2021**, *78*, 105750. [[CrossRef](#)]
121. Nie, G.; Yao, Y.; Duan, X.; Xiao, L.; Wang, S. Advances of piezoelectric nanomaterials for applications in advanced oxidation technologies. *Curr. Opin. Chem. Eng.* **2021**, *33*. [[CrossRef](#)]
122. Li, Y.-T.; Zhang, J.-J.; Li, Y.-H.; Chen, J.-L.; Du, W.-Y. Treatment of soil contaminated with petroleum hydrocarbons using activated persulfate oxidation, ultrasound, and heat: A kinetic and thermodynamic study. *Chem. Eng. J.* **2022**, *428*, 131336. [[CrossRef](#)]

123. Xu, Q.; Li, Z.; You, H.; Li, H.; Yu, Y. Foamed-Fe<sup>0</sup> via phase interface polishing by ultrasound to activate persulfate for treating triphenylmethane derivative. *J. Environ. Chem. Eng.* **2021**, *9*. [[CrossRef](#)]
124. Zhou, T.; Zou, X.; Mao, J.; Wu, X. Decomposition of sulfadiazine in a sonochemical Fe<sup>0</sup>-catalyzed persulfate system: Parameters optimizing and interferences of wastewater matrix. *Appl. Catal. B Environ.* **2016**, *185*, 31–41. [[CrossRef](#)]
125. Pan, Y.; Zhang, Y.; Zhou, M.; Cai, J.; Tian, Y. Enhanced removal of antibiotics from secondary wastewater effluents by novel UV/pre-magnetized Fe<sup>0</sup>/H<sub>2</sub>O<sub>2</sub> process. *Water Res.* **2019**, *153*, 144–159. [[CrossRef](#)] [[PubMed](#)]
126. Chakma, S.; Praneeth, S.; Moholkar, V.S. Mechanistic investigations in sono-hybrid (ultrasound/Fe<sup>2+</sup>/UVC) techniques of persulfate activation for degradation of Azorubine. *Ultrason. Sonochem.* **2017**, *38*, 652–663. [[CrossRef](#)] [[PubMed](#)]
127. Liu, J.; Zhou, J.; Ding, Z.; Zhao, Z.; Xu, X.; Fang, Z. Ultrasound irradiation enhanced heterogeneous activation of peroxydisulfate with Fe<sub>3</sub>O<sub>4</sub> for degradation of azo dye. *Ultrason. Sonochem.* **2017**, *34*, 953–959. [[CrossRef](#)]
128. Sajjadi, S.; Khataee, A.; Bagheri, N.; Kobya, M.; Senocak, A.; Demirbas, E.; Karaoglu, A.G. Degradation of diazinon pesticide using catalyzed persulfate with Fe<sub>3</sub>O<sub>4</sub>@MOF-2 nanocomposite under ultrasound irradiation. *J. Ind. Eng. Chem.* **2019**, *77*, 280–290. [[CrossRef](#)]
129. Qiu, P.; Xue, N.; Cheng, Z.; Kai, X.; Zeng, Y.; Xu, M.; Zhang, S.; Xu, C.; Liu, F.; Guo, Z. The cooperation of photothermal conversion, photocatalysis and sulfate radical-based advanced oxidation process on few-layered graphite modified graphitic carbon nitride. *Chem. Eng. J.* **2021**, *417*, 127993. [[CrossRef](#)]
130. Singh, P.; Sharma, K.; Hasija, V.; Sharma, V.; Sharma, S.; Raizada, P.; Singh, M.; Saini, A.K.; Hosseini-Bandegharaei, A.; Thakur, V.K. Systematic review on applicability of magnetic iron oxides-integrated photocatalysts for degradation of organic pollutants in water. *Mater. Today Chem.* **2019**, *14*, 100186. [[CrossRef](#)]